REDUCED ORDER STRUCTURAL MODELING OF WIND TURBINE BLADES

A Thesis

by

YELLAVENKATASUNIL JONNALAGADDA

Submitted to the Office of Graduate Studies of
Texas A&M University
in partial fulfillment of the requirements for the degree of

MASTER OF SCIENCE

August 2011

Major Subject: Aerospace Engineering

REDUCED ORDER STRUCTURAL MODELING OF WIND TURBINE BLADES

A Thesis

by

YELLAVENKATASUNIL JONNALAGADDA

Submitted to the Office of Graduate Studies of
Texas A&M University
in partial fulfillment of the requirements for the degree of

MASTER OF SCIENCE

Approved by:

Chair of Committee,	John D. Whitcomb
Committee Members,	Dimitris Lagoudas
	Anastasia Muliana
Head of Department,	Dimitris Lagoudas

August 2011

Major Subject: Aerospace Engineering

ABSTRACT

Reduced Order Structural Modeling of

Wind Turbine Blades. (August 2011)

Yellavenkatasunil Jonnalagadda, B.Tech., Indian Institute of Technology Kanpur

Chair of Advisory Committee: Dr. John D. Whitcomb

Conventional three dimensional structural analysis methods prove to be expensive for the preliminary design of wind turbine blades. However, wind turbine blades are large slender members with complex cross sections. They can be accurately modeled using beam models. The accuracy in the predictions of the structural behavior using beam models depends on the accuracy in the prediction of their effective section properties. Several techniques were proposed in the literature for predicting the effective section properties. Most of these existing techniques have limitations because of the assumptions made in their approaches.

Two generalized beam theories, Generalized Timoshenko and Generalized Euler-Bernoulli, for the static analysis based on the principles of the simple 1D-theories are developed here. Homogenization based on the strain energy equivalence principle is employed to predict the effective properties for these generalized beam theories. Two efficient methods, Quasi-3D and Unit Cell, are developed which can accurately predict the 3D deformations in beams under the six fundamental deformation modes: extension, two shears, torsion and two flexures. These methods help in predicting the effective properties using the homogenization technique. Also they can recover the detailed 3D deformations from the predictions of 1D beam analysis.

The developed tools can analyze two types of slender members 1) slender members with invariant geometric features along the length and 2) slender members with periodically varying geometric features along the length. Several configurations were

analyzed for the effective section properties and the predictions were validated using the expensive 3D analysis, strength of materials and Variational Asymptotic Beam Section Analysis (VABS). The predictions from the new tools showed excellent agreement with full 3D analysis. The predictions from the strength of materials showed disagreement in shear and torsional properties. Explanations for the same are provided recalling the assumptions made in the strength of materials approach.

To my parents

ACKNOWLEDGMENTS

It's a pleasure to thank all those who have made this research possible by sharing their knowledge and love.

I am greatly thankful to my advisor, Dr. John D. Whitcomb, for the enormous motivation and confidence that he provided to accomplish the current research work. I am thankful to the Department of Aerospace Engineering and Vestas Technology R&D Americas, Inc., for funding my graduate study and providing me with all the necessary facilities for pursuing this research.

I am thankful to the committee members, Dr. Dimitris C. Lagoudas and Dr. Anastasia Muliana, for their valuable time and advice during the review process. Also I am thankful to Dr. J. N. Reddy for accepting and lending his valuable time to be a substitute for Dr. Anastasia Muliana in her absence during the review process and the thesis defense.

I am thankful to my colleagues, Ross McLendon, Brian Owens and Kevin Maxwell, who have helped me in understanding several important concepts which formed the backbone of this research. I am thankful to Dr. Kaushik Das, a Post-Doctoral associate under Dr. Whitcomb, for the helpful discussions during the group meetings.

I owe my deepest gratitude to my parents and brother who have guided me throughout my life with their enormous love and motivation.

TABLE OF CONTENTS

CHAPTER Page

LIST OF TABLES

LIST OF FIGURES

FIGURE Page

CHAPTER I

INTRODUCTION

The wind power industry is the fastest growing among all renewable sources of energy. Efficient and robust wind turbine design techniques are required to sustain this rapid growth. A wind turbine has several components performing various functionalities, each of them playing a critical role in accounting for its efficiency. Wind turbine blades form an important structural component in wind turbines in converting the wind energy to electrical energy. The blades can cost about 20% of the total cost of the wind turbine. The efficiency of converting the wind energy to electrical energy depends on the size of the wind turbine blades. Hence the sizes of the newly designed wind turbines are increasing from day to day. The blades are slender members with the cross sectional dimensions being much smaller than their length along the axial direction. They are subjected to various loads like gravitational, aerodynamic and inertial loads under normal operational conditions.

Preliminary design of the wind turbine blades involves modeling using computational tools to perform static and dynamic analyses. This procedure can involve several design iterations during which the the blade geometry and the material properties are appropriately adjusted to meet all the design requirements. Complex cross section geometries and varying geometric features along the blade length make full 3D analysis computationally expensive. However the structural behavior of blades due to their slenderness can be accurately predicted with 1D beam models. The accuracy in the prediction using beam models depends on the degree of accuracy in the prediction of effective section properties. For static analysis the effective stiffness

---

The journal model is *IEEE Transactions on Automatic Control*.

properties need to be obtained and for dynamic analysis, in addition to the stiffness properties, effective inertial properties need to be obtained.

A. Literature Survey

The method of modeling of structural members as beams has been employed in the structural design of wind turbines for improving efficiency. Figure 1 shows a wind turbine modeled using beam elements for aeroelastic analyses. A similar approach is also used for modeling aircraft during the preliminary design stages [1]. Beam models require effective properties along with the loads acting on the structure to predict the response. There are several methods proposed in the literature to find the effective section properties for slender members of arbitrary sections. References [2] and [3] provide a brief review of the existing methods and they assess the capabilities of each of the existing methods by analyzing some example cross sections.

Most of the existing methods are based on the assumptions which simplify the analysis at the cost of accuracy. For example FAROB [4], Cross-sectional Stability of Anisotropic Blades (CROSTAB) [2] and Pre-Processor for Computing Composite Blade Properties(PreComp) [5] are based on Classical Laminate Plate Theory (CLPT). Though these methods can accurately predict the effective properties for several cross sections which meet the corresponding assumptions, they can fail when the complexity of the cross sections increase. FAROB, developed by the Dutch Knowledge Center Wind Turbine Materials and Construction, considers the cross sections as being composed of thin walled laminated flanges and calculates the section properties based on CLPT assumptions. Though FAROB is fast in obtaining the effective properties, since it is based on analytical formulations, it cannot predict the coupling behavior of blades with complex cross sections. CROSTAB, developed by the Energy

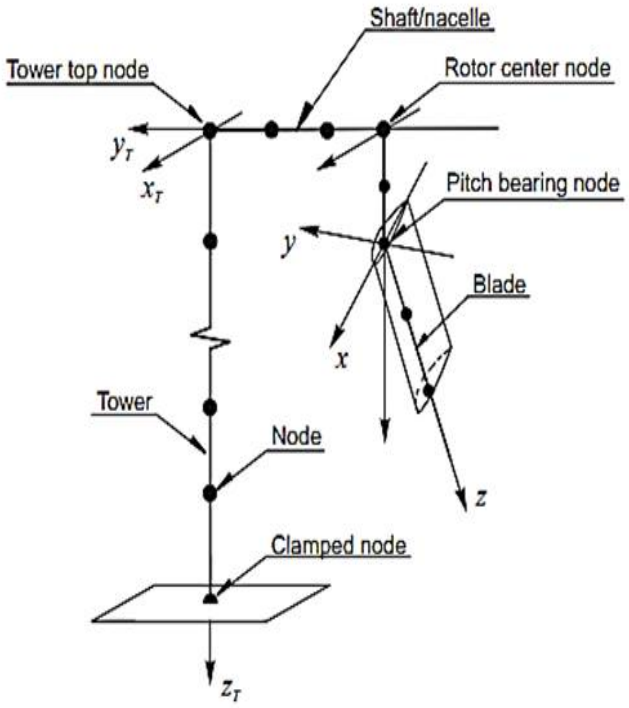

Fig. 1. Slender members modeled as beams - wind turbine [6]

Research Center of the Netherlands, also assumes the cross section being composed of thin walled layered flanges. It assumes that the flanges behave as membranes which do not contribute to the bending and torsional stiffnesses. It employs the shear flow analysis [2] to predict all the necessary effective properties, including the coupled terms, for a generalized Euler-Bernoulli beam. The limitations of CROSTAB are that it neglects the torsional and bending stiffness contributions from the flanges and moreover it cannot predict the effective shear properties. PRECOMP, developed at the National Renewable Energy Laboratory, uses a combination of CLPT and shear flow analysis. It neglects the hoop stresses in the flanges and the contributions from the shear deformation modes in calculating the effective properties.

Blade Property Extraction (BPE) [7], developed at Sandia National Laboratories, has proven to be capable of predicting all coupling behaviors for blades with general

cross sections, including the contributions from the shear modes. The method relies on 3D finite element analysis (FEA) of the full length model. The effective properties are determined by curve fitting the 3D deformation parameters to the beam deformation parameters using the least squares approach. The effective properties obtained for some cross sections using BPE were reported in reference [5] to be 50 to 60 times stiffer than the actual values. This approach is computationally expensive although it can capture the 3D details of the blades.

Variational Asymptotic Beam Section Analysis (VABS) [8], developed at Georgia Institute of Technology, is based on the Variational Asymptotic Method (VAM) which relies on expanding the strain energy functionals with respect to small parameters that are characteristic of the blade geometry (for example, aspect ratio). The formulation of VABS is complex and difficult to implement independently. This becomes a drawback if one wants to extend the approach to computationally intensive study of failure mechanics of wind turbine blades.

B. Overview of the Current Work

The objective of the current work is to develop a simple, robust and efficient method of determining the effective properties without any restrictions on the arbitrariness or the complexity of the cross sections. Also it is desired to attain the accuracy equivalent to the expensive full 3D analysis in predicting the mechanical behavior of slender members using beam models. Governing equations are derived for generalized Euler-Bernoulli and Timoshenko beam models based on equilibrium principles of linear elasticity. The Generalized Euler-Bernoulli beam model can analyze beams which exhibit couplings between extension, torsion and two flexures. It neglects the coupling behavior with the shear modes. The Generalized Timoshenko beam model

on the other hand can analyze beams which exhibit the couplings among all six fundamental deformation modes - extension, two shears, torsion and two flexures. A homogenization technique based on strain energy equivalence is employed to find the effective properties for both the beam models. The homogenization method requires the deformation fields corresponding to the fundamental deformation modes to be predicted to determine the effective properties.

The deformation fields for the fundamental modes can be obtained by analyzing a full length beam. But analyzing the full length beam can be expensive as is the case with BPE method. Two efficient methods are proposed here which can predict the deformation fields corresponding to the fundamental modes for arbitrary cross sections made of orthotropic materials. One is the Quasi-3D method which analyzes only a 2D section of the beam but assumes no coupling with shear modes. The other method is the Unit Cell method which analyzes only a small section along the length of the beam instead of the full length beam. The deformation fields obtained from these methods for various cross sections are validated using full 3D analyses. The strain energy fields corresponding to the predicted deformation fields are then utilized to predict the effective section properties using homogenization. Several cross-section shapes are analyzed and the results for effective properties are compared with the ones obtained from strength of materials (for simple cross sections), full 3D FEA and VABS. In addition, beams made of pain weave composite laminates are analyzed for transverse shear deformation behavior and effective properties. Unlike the usual prismatic slender members in which the geometry and the material distributions do not change along the length, the material distribution in plain weave composite beams varies periodically along the length. The analysis of plain weave composite beams illustrates the capability of the newly developed tools to predict mechanical behavior of slender members which have varying geometric features along the length.

CHAPTER II

THEORY

All engineering materials undergo deformations when subjected mechanical loads. The deformations are in general related to the mechanical loads applied on the material through certain characteristic properties. The deformation in most cases, to some extent, is recoverable under the removal of loads. The property of a material to be able to recover its original shape under the removal of loads is referred to as elasticity. This recoverable deformation is often referred to as elastic deformation. Most of the engineering applications which are based on the mechanical loading of materials deal with elastic deformations. Solid materials can be classified into two types based on their elastic deformations. The elastic materials in which the deformations vary linearly with the applied loads are called as linear elastic materials. The materials in which deformations do not vary linearly with the applied loads are called as nonlinear elastic materials. While many materials exhibit linear elastic behavior before the onset of plasticity (e.g. metals like iron, copper etc.), some exhibit nonlinear behavior (e.g. rubbers etc.). Structures made of linear elastic materials can also exhibit nonlinearity under large deformations. This is referred to as geometric nonlinearity. If the deformations and rotations are infinitesimal, geometric nonlinearity can be neglected. The theory of linear elasticity studies the infinitesimal elastic deformations (and infinitesimal rotations) of structures made of linear elastic materials which are under static or dynamic equilibrium when subjected to various mechanical loads.

The deformations of any three dimensional structure in general varies in all three directions. Hence a general elasticity problem is usually formulated in 3D. However, in many engineering applications the primary load bearing members are slender in shape i.e. the dimensions of such members are much larger in one direction (length)

than in the other two directions (cross section). The 3D mechanical behavior of such slender members, also called as beams, can be approximately treated as a combination of certain characteristic deformation modes. This reduces the analysis of such structures to 1D yet predicts the corresponding behavior with reasonable accuracy. The structural behavior of beams have been studied for many years and several 1D theories have been proposed in the literature. Most of the theories are developed for beams made of simple cross sections based on various characteristic deformation modes. Since the complexity of the deformation increases with the increase in the complexity of cross section, rigorous techniques are required to predict the behavior of such complex slender members for good accuracy. Two such robust theories, Generalized Euler-Bernoulli and Generalized Timoshenko beam theories, which are based on the existing simple theories are introduced in this chapter. First, the 3D linear elasticity and the simple 1D models are discussed then the two new theories are discussed in detail which can analyze slender members of any complexity. Some of the discussion in this chapter is quoted from reference [9].

A. Three-Dimensional (3D) Linear Elasticity

Consider an arbitrarily shaped body (Ω) subjected to various loads on the boundary (Γ) as shown in Figure 2. Linearized elasticity deals with finding the deformation state in the interior of the body corresponding to the applied loads at the boundary. A completely defined problem statement in linearized elasticity comprises four parts. They are equilibrium equations, kinematic relations, constitutive relations and boundary conditions (BC's). The field variables in linear elasticity are forces, displacements, stresses and strains.

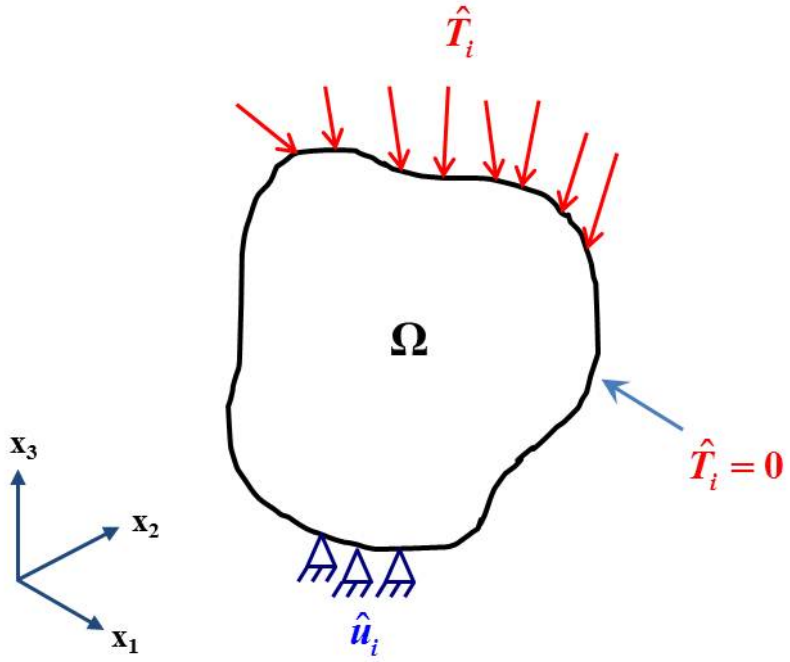

Fig. 2. Three dimensional body subjected to various loads

The equilibrium equations are given by,

$$\frac{\partial \sigma_{ij}}{\partial x_j} + f_i = 0 \qquad i, j = 1, 2, 3 \tag{2.1a}$$

$$\sigma_{ij} = \sigma_{ji} \qquad for \qquad i \neq j \tag{2.1b}$$

where f_i are the body forces. The Eq. (2.1a) corresponds to the balance of linear momentum whereas Eq. (2.1b) corresponds to the balance of angular momentum. The balance of angular momentum dictates the stress tensor to be symmetric.

The constitutive relations for a general anisotropic material based on Hooke's law are given by,

$$\sigma_{ij} = C_{ij}\varepsilon_{ij} \tag{2.2}$$

The kinematic relations which relate the engineering strains with the displace-

ments are given by,

$$\begin{aligned} \varepsilon_{ij} &= \frac{1}{2}\left(\frac{\partial u_i}{\partial x_j} + \frac{\partial u_j}{\partial x_i}\right) \qquad for \qquad i = j \\ \varepsilon_{ij} &= \left(\frac{\partial u_i}{\partial x_j} + \frac{\partial u_j}{\partial x_i}\right) \qquad for \qquad i \neq j \end{aligned} \tag{2.3}$$

Note that the engineering shear strains are used.

The boundary conditions at Γ can be specified either in terms of tractions or displacements.

$$T_i \equiv \sigma_{ji} n_j = \hat{T}_i \qquad on \qquad \Gamma_\sigma \tag{2.4a}$$

$$u_i = \hat{u}_i \qquad on \qquad \Gamma_u \tag{2.4b}$$

The above set of equations are to be solved for the unknown σ_{ij}, ε_{ij} and u_i values at each interior point of the body Ω. Also the displacements which satisfy all above equations can be shown to be unique if the following compatibility conditions are satisfied at every interior point of the body [10].

$$\begin{aligned} \frac{\partial^2 \varepsilon_{11}}{\partial {x_2}^2} + \frac{\partial^2 \varepsilon_{22}}{\partial {x_1}^2} &= \frac{\partial^2 \varepsilon_{12}}{\partial x_1 \partial x_2} \\ \frac{\partial^2 \varepsilon_{22}}{\partial {x_3}^2} + \frac{\partial^2 \varepsilon_{33}}{\partial {x_2}^2} &= \frac{\partial^2 \varepsilon_{23}}{\partial x_2 \partial x_3} \\ \frac{\partial^2 \varepsilon_{33}}{\partial {x_1}^2} + \frac{\partial^2 \varepsilon_{11}}{\partial {x_3}^2} &= \frac{\partial^2 \varepsilon_{12}}{\partial x_3 \partial x_1} \\ \frac{\partial^2 \varepsilon_{11}}{\partial x_2 \partial x_3} &= \frac{1}{2}\frac{\partial}{\partial x_1}\left(\frac{-\partial \varepsilon_{23}}{\partial x_1} + \frac{\partial \varepsilon_{31}}{\partial x_2} + \frac{\partial \varepsilon_{12}}{\partial x_3}\right) \\ \frac{\partial^2 \varepsilon_{22}}{\partial x_3 \partial x_1} &= \frac{1}{2}\frac{\partial}{\partial x_2}\left(\frac{-\partial \varepsilon_{31}}{\partial x_2} + \frac{\partial \varepsilon_{12}}{\partial x_3} + \frac{\partial \varepsilon_{23}}{\partial x_1}\right) \\ \frac{\partial^2 \varepsilon_{33}}{\partial x_1 \partial x_2} &= \frac{1}{2}\frac{\partial}{\partial x_1}\left(\frac{-\partial \varepsilon_{12}}{\partial x_3} + \frac{\partial \varepsilon_{23}}{\partial x_1} + \frac{\partial \varepsilon_{31}}{\partial x_2}\right) \end{aligned} \tag{2.5}$$

The exact solutions for the above equations in general are difficult to be obtain. In most cases, simplifying assumptions based on the nature of the problem are made

to obtain approximate closed form solutions. The 1D beam theories are some of such approaches which predict the behavior of slender members.

B. One-dimensional Theories for Simple Slender Members

Slender members are usually cylindrical in shape bound by a lateral surface and a pair of surfaces perpendicular to the lateral surface (cross sections). As mentioned previously, several simple models were proposed which can accurately predict their structural behavior. Some of the simplest models which are still being used for structural design are uniaxial extension, St. Venant's torsion, Euler-Bernoulli and Timoshenko beam models. Though these models are based on several assumptions, they demonstrate very good accuracy in predicting the behavior of slender members of simple cross sections.

The uniaxial extension theory predicts the mechanical behavior of slender members made of homogeneous material when subjected to axial loads. The theory assumes that the cross sections translate relative to adjacent ones with a constant axial displacement throughout each cross section i.e. they remain planar after the deformation. In such a case the stress state in the cross section can be shown to be with only one non-zero axial stress component σ_{11}. This model can accurately predict the behavior away from the boundaries. Figure 3 shows a schematic of slender member subjected to concentrated and distributed axial loads. Equation (2.6a) gives the equilibrium equation in terms of the resultant axial force F_1 and the distributed load f_1. The resultant axial force is related to the axial strain at each cross section of the member through the cross section property EA where E is the Young's modulus and

A is the area of the cross section. (see Eq. (2.6b)).

$$\frac{dF_1}{dx_1} + f_1 = 0 \tag{2.6a}$$

$$F_1 = EA\varepsilon_{11} \tag{2.6b}$$

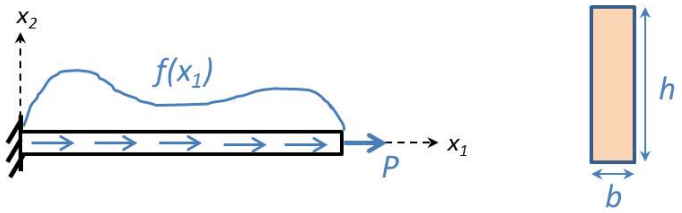

Fig. 3. Simple uniaxial extension model

The St. Venant's torsion theory analyzes slender members made of homogeneous materials which are subjected to pure torsional loads as shown in Figure 4. The solutions were first rigorously developed for beams circular cross sections and later extended for some other cross section shapes. For beams of circular cross sections, from symmetry arguments the theory assumes that cross section planes remain planar and rotate about the axis along length relative to the adjacent cross section planes. For slender members of non-circular cross sections, the cross section planes rotate relative to each other but do not remain planar and tend to warp in the axial direction. This warping displacement, however, remains constant for all cross sections if the rate of twist is constant. The theory predicts only two non-zero stress components, σ_{12} and σ_{13}, and all other components are zero throughout the slender member [8]. The equilibrium condition is given by Eq. (2.7a) in terms of the resultant torque M_1 and the distributed moment m_1. The resultant torque is related to the rate of twist, κ_1, as given by Eq. (2.7b). Here D is called the torsional rigidity of the cross section. For circular cross section D can be shown to be equal to GJ where G is the shear

modulus and J is the polar moment of area of the cross section.

$$\frac{dM_1}{dx_1} + m_1 = 0 \tag{2.7a}$$

$$M_1 = D\kappa_1 \tag{2.7b}$$

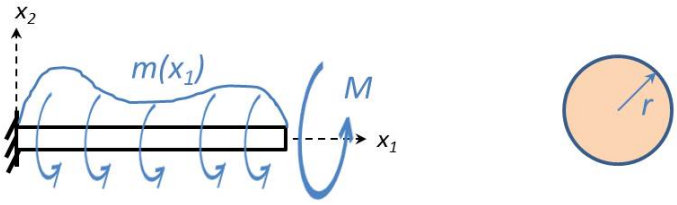

Fig. 4. St. Venant's torsion model

The Euler-Bernoulli beam theory analyzes the behavior of slender members made of homogeneous material subjected to transverse loads and bending moments. Figure 5 shows a schematic of a beam subjected to transverse loads and bending moments. The theory assumes that the beam is made of several longitudinal fibers bundled together. Under pure bending, the theory assumes that the plane sections remain planar and rotate normal to the neutral axis. This assumption leads to a zero transverse shear strain in each cross section. The only non-zero component under these assumptions is the axial stress σ_{11}. The equilibrium conditions are given by Eqs. (2.8a) and (2.8b). Here, F_3 is the resultant transverse shear force, M_2 is the resultant bending moment and f_3 and m_3 are the applied distributed forces and moments respectively. The Eq. (2.8c) relates the resultant bending moment M_2 and the bending curvature κ_2 through the cross section property, EI_{22}. Here E is the Young's modulus and I_{22}

is the second moment of area about x_2.

$$\frac{dF_3}{dx_1} + f_3 = 0 \tag{2.8a}$$

$$\frac{dM_2}{dx_1} - F_3 + m_2 = 0 \tag{2.8b}$$

$$M_2 = EI_{22}\kappa_2 \tag{2.8c}$$

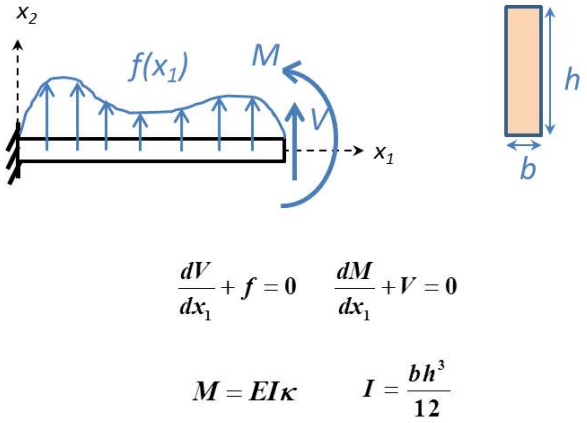

Fig. 5. Euler-Bernoulli beam model

The Euler-Bernoulli beam theory can accurately predict the behavior of slender members which are of large aspect ratios i.e. the ratio of length to the cross sectional dimensions. But for the slender members with smaller aspect ratios the shear strain can be significant and cannot be neglected. The Timoshenko beam theory which also addresses the problem of beam bending considers the transverse shear strain to be non-zero and uniform in each cross section (see Figure 6). In general the shear strain in each cross section follows a complex distribution depending on the cross section shape and material properties. In addition to Eqs. (2.8) which are also valid for the Timoshenko beam theory, the cross section property relation corresponding to the shear resultant must be considered. The shear resultant F_3 is related to the average

transverse shear strain ϵ_{13} in each cross section as,

$$F_3 = KGA\gamma_{13} \tag{2.9}$$

where K is the shear correction factor which accounts for the non-uniform shear strain in the actual slender member and G is the shear modulus.

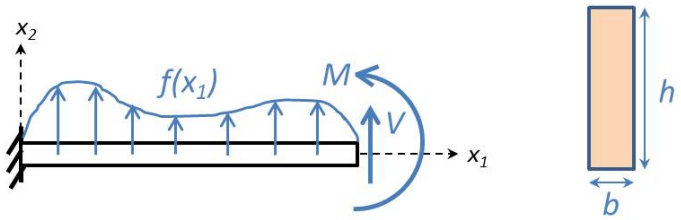

$$\frac{dV}{dx_1} + f = 0 \qquad \frac{dM}{dx_1} + V = 0$$

$$M = EI\frac{d\phi}{dx_1} \qquad V = KGA\left(\phi - \frac{du_2}{dx_1}\right)$$

$$I = \frac{bh^3}{12} \qquad A = bh$$

Fig. 6. Timoshenko beam model

Each of the simple models described above are based on assumptions on the nature of deformation, material property and the loading conditions. Note that there is one common assumption for all the above theories. The common assumption is that the lateral surfaces of the beam are traction free and the stress components σ_{22}, σ_{33} and σ_{23} are zero throughout the beam. Since these theories were initially developed for homogeneous beams, this assumptions turn out to be valid in most cases. However if they are extended to analyze inhomogeneous beams as discussed in [11], the stress components σ_{22}, σ_{33} and σ_{23} can be non-zero at the interface of two different materials. The equilibrium and compatibility conditions of elasticity dictate that the tractions and displacements on the interface between two different

materials must be continuous. If the materials have different Poisson's ratios, these conditions can lead to non-zero inter facial stresses. Additional equations are required to account for such a behavior of inhomogeneous beams which the above mentioned simple models fail to address. Also these simple models can fail if the material anisotropy leads to deformations in which the cross section planes do not remain planar under extension and flexure modes. This can happen if the beams are made of angled unidirectional composite plies. The wind turbine blades are usually made of different layups of composite materials and their distribution is not uniform in each cross section. In general such complex blades exhibit coupling between different fundamental deformation modes (extension, shears, torsion and flexures) in beams. To analyze such complex cross sections, two generalized beam theories are developed here based on the principles of the simple theories. The generalized theories which are discussed in detail in the next section, employ the finite element analysis (FEA) tools to enforce all required continuity conditions and predict the detailed stress distributions in beams with accuracy equivalent to full 3D analysis. Note that all these simple models were developed making predictions away from the boundaries of the slender member.

C. Generalized Beam Theories

The two generalized theories which are formulated in this section are Generalized Euler-Bernoulli and Generalized Timoshenko beam theories. The generalized Euler-Bernoulli theory neglects the contributions from transverse shear strains (like the corresponding simple theory) whereas the generalized Timoshenko considers the transverse shear strains to be significant. Both the theories extend the principles of the simple theories presented in the previous section to analyze slender members of any

arbitrary cross sections (including the ones which show coupling among the fundamental modes) subjected to any combination of forces and moments (see Figure 7). First the governing equations are developed for the Generalized Timoshenko beam, i.e. considering the shear strain to be non-zero. The governing equations for the Generalized Euler-Bernoulli beam are then developed as a special case of Generalized Timoshenko beam by considering the transverse shear strains to be zero.

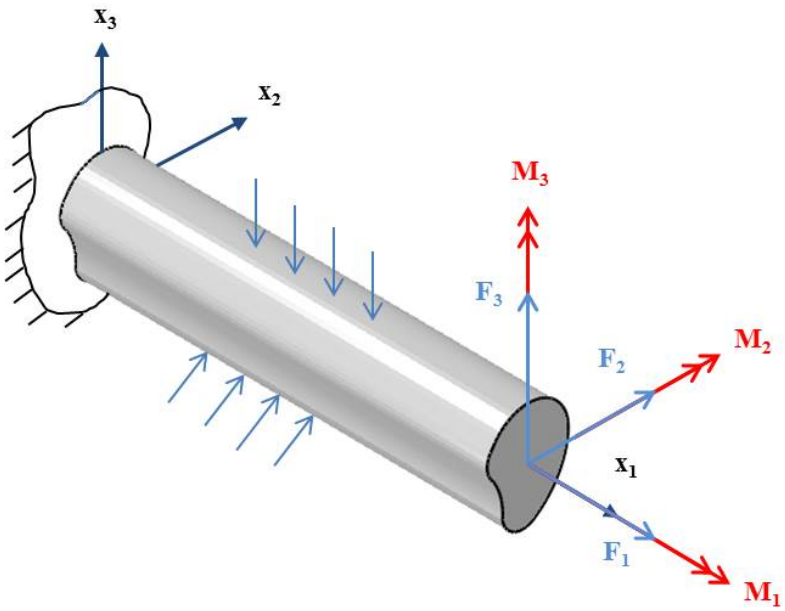

Fig. 7. Generalized beam model

1. Generalized Timoshenko Beam Theory

a. Kinematic Relations

The kinematic relations relate the six generalized strains, e_i, of the beam which include axial strain (ϵ_1), two shear strains (γ_{12} and γ_{13}), rate of twist (κ_1) and two flexural curvatures (κ_2 and κ_3), with the displacements (v_i) of the beam reference axis and rotations (ϕ_i) of the cross section planes about the reference axis. Equation (2.10)

gives the kinematic relations for the generalized Timoshenko beam. The transverse shear strains, γ_{12} and γ_{13}, are defined according to the simple Timoshenko beam theory, in terms of the transverse displacements v_2, v_3 and rotations ϕ_2, ϕ_3.

$$\begin{aligned} e_1 &= \varepsilon_{11} = \frac{dv_1}{dx_1} \\ e_2 &= \gamma_{12} = -\phi_3 + \frac{dv_2}{dx_1} \\ e_3 &= \gamma_{13} = \phi_2 + \frac{dv_3}{dx_1} \\ e_4 &= \kappa_1 = \frac{d\phi_1}{dx_1} \\ e_5 &= \kappa_2 = \frac{d\phi_2}{dx_1} \\ e_6 &= \kappa_3 = \frac{d\phi_3}{dx_1} \end{aligned} \tag{2.10}$$

where the beam displacements v_i and rotations ϕ_i are given by,

$$\begin{aligned} v_1 &= u_1\left(x_1, 0, 0\right) \\ v_2 &= u_2\left(x_1, 0, 0\right) \\ v_3 &= u_3\left(x_1, 0, 0\right) \\ \phi_1 &= \frac{\partial u_3}{\partial x_2}\left(x_1, x_2, x_3\right) - \frac{\partial u_2}{\partial x_3}\left(x_1, x_2, x_3\right) \\ \phi_2 &= \frac{\partial u_1}{\partial x_3}\left(x_1, x_2, x_3\right) \\ \phi_3 &= -\frac{\partial u_1}{\partial x_2}\left(x_1, x_2, x_3\right) \end{aligned} \tag{2.11}$$

Note that under pure torsion and flexure modes in cross sections made of orthotropic materials, the rotations ϕ_i do not vary with x_2 and x_3.

b. Stress Resultants

The six stress resultants, R_i, which include an axial force (F_1), two shear forces (F_2 and F_3) and one torque (M_1) and two bending moments (M_2 and M_3) are related

to the stresses in each cross section as given in Eq. (2.12). Figure (8) shows the positive directions of the stress resultants indicating the sign conventions used for the formulation. Note that the resultants are left in the integral form unlike the simple theories, since the distribution of stresses on the cross section planes are unknown for slender members of arbitrary cross sections.

$$
\begin{aligned}
R_1 = F_1 &= \int_A \sigma_{11} dA \\
R_2 = F_2 &= \int_A \sigma_{12} dA \\
R_3 = F_3 &= \int_A \sigma_{13} dA \\
R_4 = M_1 &= \int_A \left(\sigma_{13} x_2 - \sigma_{12} x_3\right) dA \\
R_5 = M_2 &= \int_A \sigma_{11} x_3 dA \\
R_6 = M_3 &= -\int_A \sigma_{11} x_2 dA
\end{aligned}
\tag{2.12}
$$

c. Equilibrium Equations

The differential form of equilibrium equations for the generalized beam shown in Figure (7) can derived by considering the equilibrium of an infinitesimal element along length of the beam. Considering that the beam is loaded with distributed forces (f_i) and moments (m_i) along the length, the equilibrium conditions are given

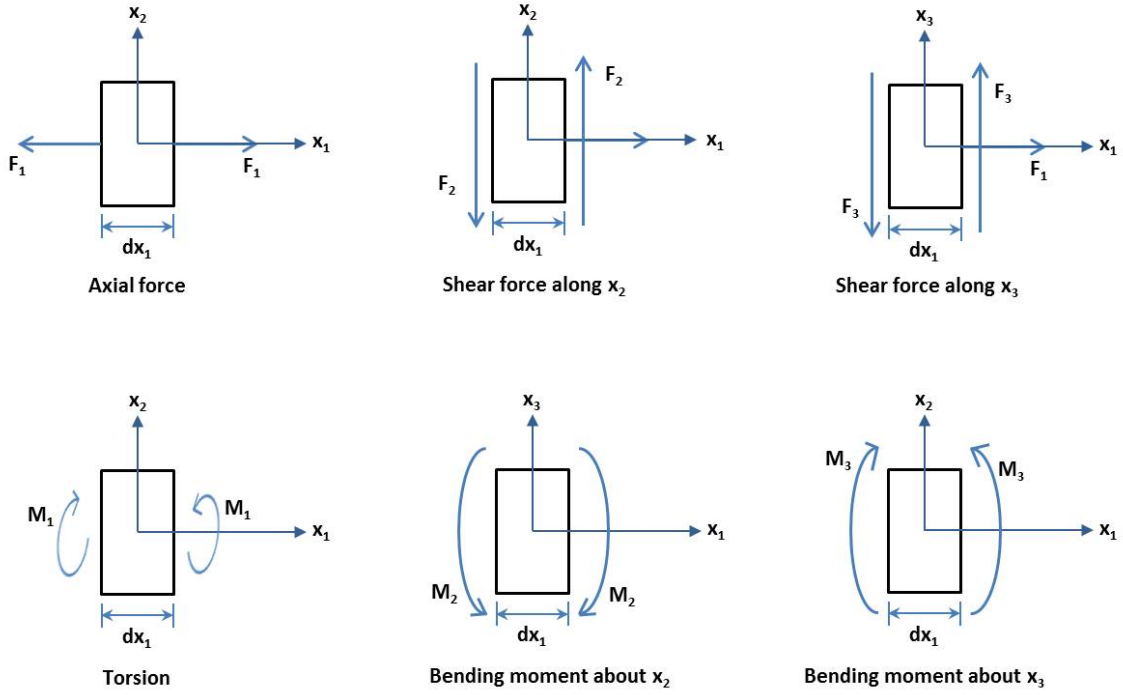

Fig. 8. Positive directions of the six stress resultants indicating the sign convention used for the generalized beam formulation

by,

$$\begin{aligned} \frac{dF_1}{dx_1} + f_1 &= 0 \\ \frac{dF_2}{dx_1} + f_2 &= 0 \\ \frac{dF_3}{dx_1} + f_3 &= 0 \\ \frac{dM_1}{dx_1} + m_1 &= 0 \\ \frac{dM_2}{dx_1} - F_3 + m_2 &= 0 \\ \frac{dM_3}{dx_1} + F_2 + m_3 &= 0 \end{aligned} \tag{2.13}$$

d. Effective Properties

The stress resultants in the simple theories are related to the corresponding generalized strains through the cross section properties EA, KGA, GJ and EI_{22}. These properties were derived assuming the beams exhibit no coupling among extension, shear, torsion and flexures. If a beam exhibits coupled behavior, one stress resultant can lead to more than one deformation mode (i.e. more than one non-zero generalized strain e_i). To represent all possible coupling behaviors in a general beam, the six stress resultants are related to the six generalized strains by Eq. (2.14).

$$R_i = C_{ij} e_j \qquad i, j = 1 \ldots 6 \tag{2.14}$$

where C_{ij} are the beam effective properties. The Eq. (2.14) for homogeneous beam of solid cross section showing no coupling behavior is,

$$\begin{Bmatrix} F_1 \\ F_2 \\ F_3 \\ M_1 \\ M_2 \\ M_3 \end{Bmatrix} = \begin{bmatrix} EA & 0 & 0 & 0 & 0 & 0 \\ 0 & K_2GA & 0 & 0 & 0 & 0 \\ 0 & 0 & K_3GA & 0 & 0 & 0 \\ 0 & 0 & 0 & GJ & 0 & 0 \\ 0 & 0 & 0 & 0 & EI_{22} & 0 \\ 0 & 0 & 0 & 0 & 0 & EI_{33} \end{bmatrix} \begin{Bmatrix} \epsilon_1 \\ \epsilon_2 \\ \epsilon_3 \\ \kappa_1 \\ \kappa_2 \\ \kappa_3 \end{Bmatrix} \tag{2.15}$$

However, for complex cross sections such as in wind turbine blades, the matrix C_{ij} can be fully populated.

2. Generalized Euler-Bernoulli Beam Theory

The governing equations for the generalized Euler-Bernoulli beam can be obtained as special case of the generalized Timoshenko beam model by considering the transverse shear strains at each cross section to be zero. This implies, from the kinematic

relations given in Eq. (2.10), the rotations ϕ_2 and ϕ_3 must be equal to the displacement gradients $-\frac{dv_3}{dx_1}$ and $\frac{dv_2}{dx_1}$ respectively. The kinematic relations for the flexural curvatures, κ_2 and κ_3 are then given by Eq. (2.16).

$$\begin{aligned} e_5 = \kappa_2 &= -\frac{d^2 v_3}{{dx_1}^2} \\ e_6 = \kappa_3 &= \frac{d^2 v_2}{{dx_1}^2} \end{aligned} \tag{2.16}$$

The definition of stress resultants and the equilibrium equations given in Eqs. (2.12) and (2.13) respectively are still valid for the generalized Euler-Bernoulli beam. However, the effective properties correspond to only four resultants and four generalized strains which are given by Eq. (2.17).

$$R_i = C_{ij} e_j \qquad i, j = 1, 4, 5 \; and \; 6 \tag{2.17}$$

Note that the effective properties in the simple theories were obtained easily because the corresponding assumptions led to simple stress distributions in the cross section which in most cases can be obtained in closed form. But for beam of arbitrary cross sections, such closed form solutions are difficult to obtain and hence a robust approach is needed to extract the effective properties. One such approach is described in the next section based on the homogenization principles.

D. Homogenization Method for Determining the Effective Properties

Engineering materials with complex micro structure subjected to even simple loads can exhibit complex distribution of stresses and strains internally. But the global average response of the same material can be simple if the applied loads do not vary severely over the material space. Also the prediction of detailed internal stresses and strains is not required for most of the applications. Hence "effective properties"

which relate the average response to the applied loads are often defined to reduce the effort in making predictions of the mechanical behavior. Homogenization in elasticity refers to predicting these effective properties based on the strain energy equivalence principle. The principle states that the strain energy of the complex body should be equal to that of the equivalent homogenized body. Reasonable accuracy can be achieved in the predictions of mechanical behavior using effective properties if the irregularities in the original micro structure are not severe.

In the current problem of beam-like modeling of wind turbine blades, the principle of strain energy equivalence states that the strain energy of the 3D slender member when subjected to any arbitrary loading should be equal to the strain energy of the equivalent beam when subjected to the same loading. Here, the complex cross section is homogenized to predict the effective properties required for beam-like modeling. Homogenization based on strain energy equivalence has been employed previously by [12] and [13] but the approaches were not sufficiently rigorous to predict the full C_{ij} matrix.

If a 3D slender member is subjected to a specific loading, then the corresponding strain energy is calculated in terms of the 3D stresses and strains as given by Eq. (2.18),

$$U_{3D} = \frac{1}{2} \int_V \sigma_{ij} \varepsilon_{ij} dV \tag{2.18}$$

If the same loading generates the stress resultants R_i and the generalized strains e_j in the equivalent beam, then the strain energy is given by Eq. (2.19).

$$U_B = \frac{1}{2} \int_0^L R_i e_i dx_1 = \frac{1}{2} \int_0^L R_i R_j S_{ij} dx_1 \tag{2.19}$$

where S_{ij} are the effective compliance properties of the slender member. According to the strain energy equivalence principle, on equating the strain energies given in

Eqs. (2.18) and (2.19), a relation in terms of the unknown S_{ij} is obtained as follows

$$\frac{1}{2}\int_0^L R_i R_j S_{ij} dx_1 = \frac{1}{2}\int_V \sigma_{ij}\varepsilon_{ij} dV \tag{2.20}$$

Note that the stress resultants, R_i, in Eq. (2.20) can be obtained from the 3D analysis of the slender member using the Eq. (2.12). The only unknowns in the Eq. (2.20) are the effective properties S_{ij}. Hence if the detailed 3D deformations corresponding to 21 independent loading cases which give relations like Eq. (2.20) are known, the fully populated symmetric effective compliance matrix S_{ij} can be determined completely. Because of S_{ij} being symmetric, it has only 21 unknowns. To establish the required relations, there are two tasks to be performed. One is to determine what these 21 independent load cases should be and the second is to obtain the 3D deformations for all those load cases.

Note that the beam strain energy in Eq. (2.20) is quadratic in terms of the stress resultants, R_i. Hence the 21 independent load cases can be considered as linear combinations of the six fundamental modes as shown in Eq. (2.21).

$$(R_i + R_j) \;\; i = 1, 6 \text{ and } j = i, 6 \tag{2.21}$$

The 3D solutions corresponding to the six fundamental load cases should not have any end effects i.e. the deformations should correspond to the interior of a long 3D slender member which do not depend on how the loads are applied at the boundaries. The Saint-Venant's principle ensures us that such deformations exist considerable away from the ends of the beam. To avoid the end effects in calculating the strain energies, the 3D deformations can be considered from only the interior of a long beam model where the influence of the end effects is minimal. The solutions for the long beam can be obtained by employing 3D FEA of linear elasticity. However this

approach can be expensive, especially if the complexity of the cross section geometry and material distributions increase. Since the deformations from only the interior of the long beam are required, the computational time can be significantly reduced if those deformations can be predicted by analyzing only the interior region instead of the full length long beam. Two such methods are developed here which can predict the 3D deformations corresponding to the fundamental modes by analyzing just a small section of the full length model.

The first method is the Quasi-3D method which can predict the detailed 3D deformations of slender members subjected to extension, torsion and flexures by analyzing just a 2D section of the full length model. The Quasi-3D method neglects the contributions from shear strains and assumes that the slender member does not show any coupling behavior with the shear modes. The second method is the Unit Cell method which can predict the detailed 3D deformations of slender members when subjected to any combinations of the six fundamental modes. The Unit Cell method includes the contributions from the shear deformations and hence it can also analyze cross sections which show coupling with the shear modes.

E. Quasi-3D (Q3D) Method

The term Quasi-3D (Q3D) in elasticity refers to a deformation which does not vary in one of the 3 dimensions. The deformations in slender members which do not show any coupling with the shear modes, remains constant along the length when subjected to extension, torsion and/or flexure. Figure 9 shows flexure and torsion modes of a 3-cell homogeneous thin walled box beam. The stress contours can be seen to be invariant along the axial direction x_1. The contours (deformation) vary only in the plane of the cross section. Hence these modes are referred to as Q3D deformation

modes. If one can predict the detailed stresses and strains in one cross section, then complete deformation of the full length model is known.

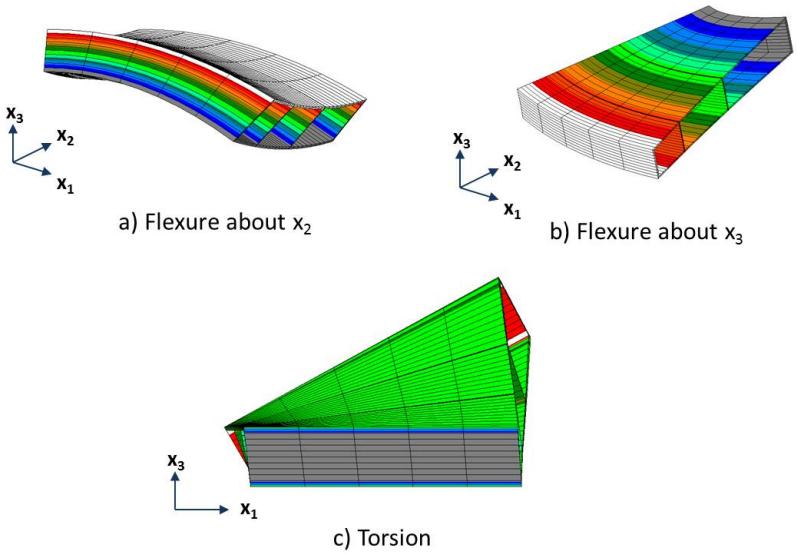

Fig. 9. Quasi-3D deformations in beams

Consider the Taylor's series expansion of the 3D displacements up to second order about the origin of the coordinate system as follows,

$$u_i = u_i|_{x_i=0} + \left.\frac{\partial u_i}{\partial x_j}\right|_{x_i=0} x_j + \frac{1}{2}\left.\frac{\partial^2 u_i}{\partial x_j \partial x_k}\right|_{x_i=0} x_j x_k + \text{h.o.t} \tag{2.22}$$

If all the terms that vary only with x_2 and/or x_3 are grouped together with the higher order terms (h.o.t), then

$$\begin{aligned}
u_1 &= u_1|_{x_i=0} + \left.\frac{\partial u_1}{\partial x_1}\right|_{x_i=0} x_1 + \left.\frac{\partial^2 u_1}{\partial x_1 \partial x_2}\right|_{x_i=0} x_1 x_2 + \left.\frac{\partial^2 u_1}{\partial x_1 \partial x_3}\right|_{x_i=0} x_1 x_3 + U_1(x_2, x_3) \\
u_2 &= u_2|_{x_i=0} + \left.\frac{\partial u_2}{\partial x_1}\right|_{x_i=0} x_1 + \frac{1}{2}\left.\frac{\partial^2 u_2}{\partial {x_1}^2}\right|_{x_i=0} {x_1}^2 + \left.\frac{\partial^2 u_2}{\partial x_3 \partial x_1}\right|_{x_i=0} x_3 x_1 + U_2(x_2, x_3) \\
u_3 &= u_3|_{x_i=0} + \left.\frac{\partial u_3}{\partial x_1}\right|_{x_i=0} x_1 + \frac{1}{2}\left.\frac{\partial^2 u_3}{\partial {x_1}^2}\right|_{x_i=0} {x_1}^2 + \left.\frac{\partial^2 u_3}{\partial x_2 \partial x_1}\right|_{x_i=0} x_2 x_1 + U_3(x_2, x_3)
\end{aligned} \tag{2.23}$$

where U_i do not depend on x_1 and represent the variation of displacements in the plane of the cross section. If the slender member is constrained for rigid body translations at origin, then the terms (u_i^0) vanish. On assuming the transverse shear strains to be zero, the terms $\frac{\partial u_2}{\partial x_1}$ and $\frac{\partial u_3}{\partial x_1}$ also vanish. Under pure extension, torsion and flexures the corresponding generalized strains ϵ_1, κ_1, κ_2 and κ_3 remain constant throughout the slender member. Hence, by using the Eqs. (2.10) and (2.16) in Eq. (2.23) the 3D displacements in the slender members take the following form,

$$\begin{aligned} u_1(x_1, x_2, x_3) &= \epsilon_1 x_1 + \kappa_2 x_1 x_3 - \kappa_3 x_1 x_2 + U_1(x_2, x_3) \\ u_2(x_1, x_2, x_3) &= \frac{1}{2}\kappa_3 x_1^2 - \kappa_1 x_1 x_3 + U_2(x_2, x_3) \\ u_3(x_1, x_2, x_3) &= -\frac{1}{2}\kappa_2 x_1^2 + \kappa_1 x_1 x_2 + U_3(x_2, x_3) \end{aligned} \tag{2.24}$$

Using the definition of linearized strains from elasticity theory given in Eq. (2.3), the 3D strains ε_{ij} in terms of the beam generalized strains can be obtained as follows,

$$\begin{aligned} \varepsilon_{11}(x_1, x_2, x_3) &= \frac{\partial u_1}{\partial x_1} = \epsilon_1 + \kappa_2 x_3 - \kappa_3 x_2 \\ \varepsilon_{22}(x_1, x_2, x_3) &= \frac{\partial u_2}{\partial x_2} = \frac{\partial U_2(x_2, x_3)}{\partial x_2} \\ \varepsilon_{33}(x_1, x_2, x_3) &= \frac{\partial u_3}{\partial x_3} = \frac{\partial U_3(x_2, x_3)}{\partial x_3} \\ 2\varepsilon_{23}(x_1, x_2, x_3) &= \frac{\partial u_2}{\partial x_3} + \frac{\partial u_3}{\partial x_2} = \frac{\partial U_2(x_2, x_3)}{\partial x_3} + \frac{\partial U_3(x_2, x_3)}{\partial x_2} \\ 2\varepsilon_{13}(x_1, x_2, x_3) &= \frac{\partial u_1}{\partial x_3} + \frac{\partial u_3}{\partial x_1} = \frac{\partial U_1(x_2, x_3)}{\partial x_3} + \kappa_1 x_2 \\ 2\varepsilon_{12}(x_1, x_2, x_3) &= \frac{\partial u_1}{\partial x_2} + \frac{\partial u_2}{\partial x_1} = \frac{\partial U_1(x_2, x_3)}{\partial x_2} - \kappa_1 x_3 \end{aligned} \tag{2.25}$$

Note that the 3D strains in Eq. (2.25) do not depend on x_1 and hence illustrate that the q3D deformations remain constant along the length of the slender member. The in-plane variation of displacements, U_i need to be evaluated to predict the 3D strains throughout the slender member. This in-plane variation of displacements can

be predicted using finite element analysis of a 2D mesh of the cross section. The detailed Q3D finite element formulation is derived in the next chapter.

F. Unit Cell Method

The Quasi-3D method can only capture the deformations which do not change along the length of the slender member. When there is shear, the deformation varies along the length. This is because of the shear-flexure coupling that arises from the beam equilibrium. Equation (2.13) states that under the absence of distributed loads (f_i and m_i), a constant shear resultant (F_2 or F_3) exists throughout the beam. This constant shear resultant generates a linearly varying moment (M_3 or M_2) along x_1 (also from equilibrium) which results in the variation of the deformation along x_1. Hence the deformation under a constant shear resultant can no more be classified as Quasi-3D behavior.

To predict the effective shear properties by the corresponding 3D deformations need to be evaluated. One can always analyze a full length beam and use the deformations away from the ends. As mentioned previously, it can be very expensive approach for complex cross sections. Instead one can analyze a small section along the length of the slender member, which is referred to as "Unit Cell"(see Figure 10) in the following discussion. By applying appropriate boundary conditions on the unit cell, the shear deformation mode can be captured. The boundary conditions must not induce any end effects in the unit cell.

1. BCs for Extension, Torsion, and Flexure Modes

The deformations under pure extension, torsion and flexure modes, do not change along the length of the slender member even if the cross section exhibits coupling

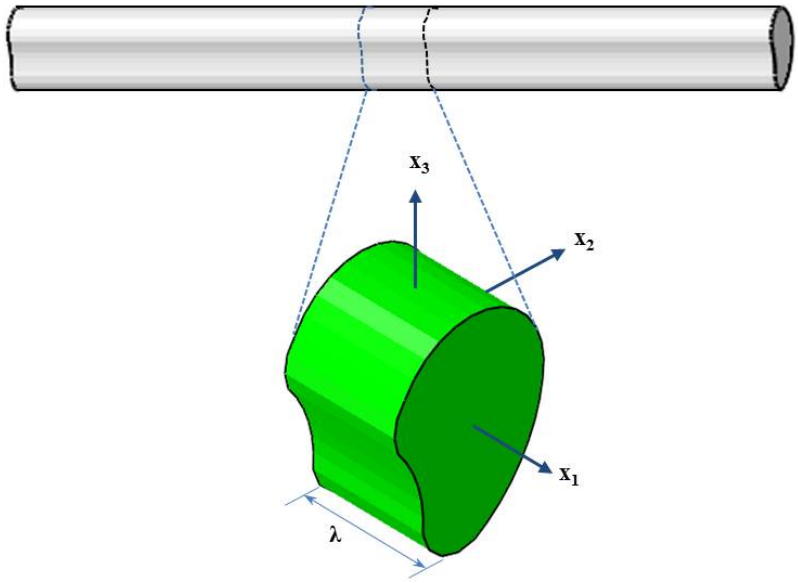

Fig. 10. Unit cell for a slender member with arbitrary cross section

with shear modes. This is because under pure extension, torsion or flexure, from the equilibrium equations, the stress resultants do not vary along the length. A pure mode here is defined as the deformation state in which only the corresponding resultant force or moment is non-zero. For example, the pure extension mode corresponds to the deformation state in which only the axial force F_1 is non-zero. Also, if the unit cell of the slender member exhibits symmetry (geometry and material distribution) about the x_2x_3 plane, the cross section remains planar under these four deformation modes. Hence the boundary conditions for such unit cells can be imposed as plane translations and rotations of the end cross section planes.

BC's for extension are,

$$\begin{aligned} u_1\left(-\frac{\lambda}{2}, x_2, x_3\right) &= -c \qquad u_1\left(\frac{\lambda}{2}, x_2, x_3\right) = c \\ T_i\left(\pm\frac{\lambda}{2}, x_2, x_3\right) &= 0 \qquad i = 2, 3 \end{aligned} \tag{2.26}$$

BC's for torsion are,

$$\begin{aligned} &u_2\left(-\frac{\lambda}{2}, x_2, x_3\right) = c * x_3 \qquad u_3\left(-\frac{\lambda}{2}, x_2, x_3\right) = -c * x_2 \\ &u_2\left(\frac{\lambda}{2}, x_2, x_3\right) = -c * x_3 \qquad u_3\left(\frac{\lambda}{2}, x_2, x_3\right) = c * x_2 \\ &T_1\left(\pm\frac{\lambda}{2}, x_2, x_3\right) = 0 \end{aligned} \tag{2.27}$$

BC's for flexure about x_2 are,

$$\begin{aligned} &u_1\left(-\frac{\lambda}{2}, x_2, x_3\right) = -c * x_3 \qquad u_1\left(\frac{\lambda}{2}, x_2, x_3\right) = c * x_3 \\ &T_i\left(\pm\frac{\lambda}{2}, x_2, x_3\right) = 0 \qquad i = 2, 3 \end{aligned} \tag{2.28}$$

BC's for flexure about x_3 are,

$$\begin{aligned} &u_1\left(-\frac{\lambda}{2}, x_2, x_3\right) = c * x_2 \qquad u_1\left(\frac{\lambda}{2}, x_2, x_3\right) = -c * x_2 \\ &T_i\left(\pm\frac{\lambda}{2}, x_2, x_3\right) = 0 \qquad i = 2, 3 \end{aligned} \tag{2.29}$$

where c can be any non-zero constant. Note that in all the above four cases, the lateral surfaces are left traction free.

2. Shear Modes in Beams

Unlike pure extension, torsion and flexure modes, a pure shear mode does not exist in beams. As mentioned earlier, a constant shear resultant generates a linearly varying moment along the length. Hence the deformation does not exhibit symmetry about the x_2x_3 plane, even if the geometry and the material properties do exhibit a mirror symmetry about x_2x_3 plane. This implies the cross section planes do not remain planar and tend to warp under a constant shear resultant. Hence the required BCs for shear modes should accommodate for free warping of the cross section planes. Otherwise stress concentrations arise in the unit cell which can lead to incorrect

predictions of the corresponding strain energies.

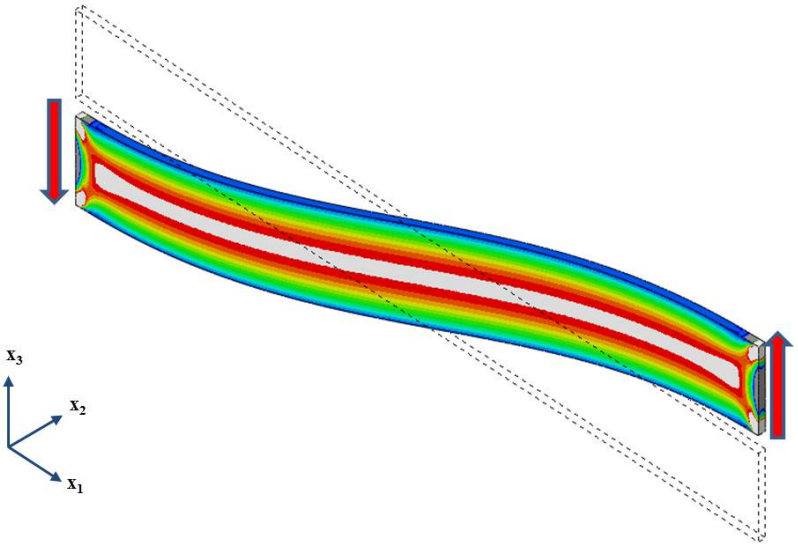

Fig. 11. Full length beam under end shear loads showing end effects

To illustrate the extent of end effects that arise on constraining the warping, Figure 11 shows the deformation of a full length homogeneous beam with rectangular cross section made of isotropic material subjected to plane translation BCs (i.e. $u_1 = 0$ and $u_3 =$ constant at the end cross section planes). The figure shows σ_{13} contours in the beam. It can be noticed that the shear stress contours are uniform along the length away from the ends. But near the ends where the BCs are applied, the contours are not uniform and varied drastically. This is because of the effect of constrained warping. The end effects vanish after a certain distance away from the ends in accordance with the Saint-Venant's principle, but it is significant near the ends. The end effects are more pronounced if the same plane translation BCs are applied on a unit cell of short length as illustrated in Figure 12. Hence it is necessary to derive the correct BCs for unit cell i.e. the BCs which do not constrain warping of the cross sections. A method based on the superposition principle of elasticity was developed and is discussed in the next section.

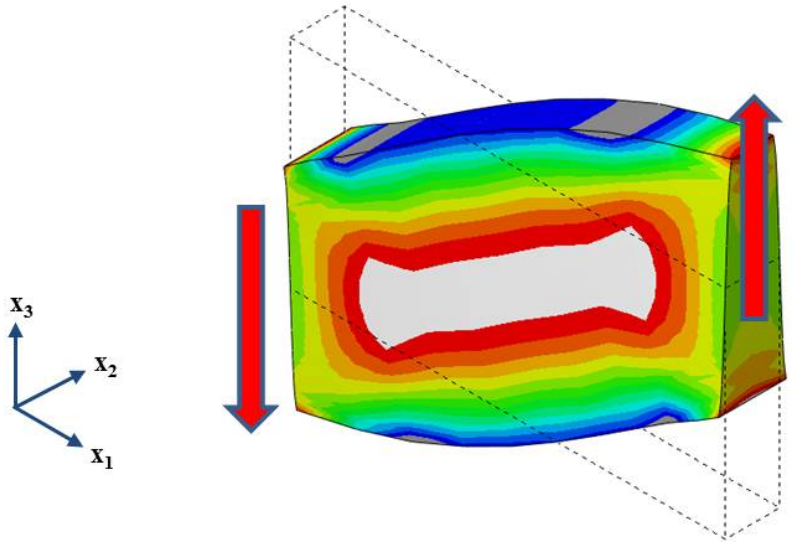

Fig. 12. Unit cell with under plane translation BCs showing end effects

3. Superposition Method for Derivation of BCs for Shear Modes

The superposition method uses the basic principle of superposition in linear elasticity to obtain relations between the deformations in adjacent unit cells in the long beam. Then it employs the Equivalent Coordinate System (ECS) relations [14] to obtain the relation between displacements and tractions on the either end faces of center unit cell in terms of the known solution for uniform flexure.

a. Superposition Relations Using the Superposition Principle of Linear Elasticity

Consider a full length beam model being subjected to end shear loads, V as shown in Figure 13. This loading generates a constant shear resultant F_3 equal to V and a linearly varying moment M_3 in the beam. If the beam is considered to be divided in to several unit cells each of length λ along the length of the beam, then the shear resultant would be a constant equal to V in all unit cells. Since the moment varies linearly, the difference in the moment resultants acting on adjacent unit cells would be

a constant equal to λV. This implies the deformation in one unit cell can be obtained from that in the adjacent unit cell by superposing it with the solution corresponding to the constant moment equal to λV.

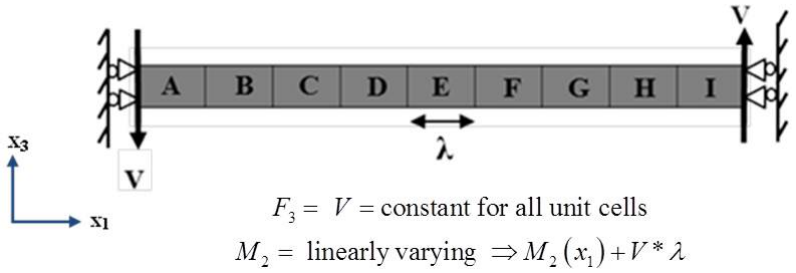

Fig. 13. Loads in each unit cell of a beam subjected to end shear loads

Consider the displacement gradients corresponding to adjacent unit cells in the full length beam. Using the superposition principle they are related as,

$$\frac{\partial u_i}{\partial x_j}(x_1+\lambda, x_2, x_3) = \frac{\partial u_i}{\partial x_j}(x_1, x_2, x_3) + \frac{\partial \hat{u}_i}{\partial x_j}(x_1, x_2, x_3) \qquad i,j = 1,2,3 \qquad (2.30)$$

where $\hat{u}_i$ correspond to the deformation in the unit cell under a constant moment. To obtain the relation between the gradients on the end faces of the center unit cell, substitute $x_1 = -\frac{\lambda}{2}$.

$$\frac{\partial u_i}{\partial x_j}\left(\frac{\lambda}{2}, x_2, x_3\right) = \frac{\partial u_i}{\partial x_j}\left(-\frac{\lambda}{2}, x_2, x_3\right) + \frac{\partial \hat{u}_i}{\partial x_j}\left(-\frac{\lambda}{2}, x_2, x_3\right) \qquad i,j = 1,2,3 \quad (2.31)$$

The superposition relations similar to the ones in terms of displacement gradients given in Eq. (2.30), also can be obtained for stresses as follows,

$$\sigma_{ij}(x_1+\lambda, x_2, x_3) = \sigma_{ij}(x_1, x_2, x_3) + \hat{\sigma}_{ij}(x_1, x_2, x_3) \;\; i,\; j \;=\; 1,\; 2,\; 3 \qquad (2.32)$$

where $\hat{\sigma_{ij}}$ corresponds to the constant moment solution.

The Eqs. (2.31) and (2.32) alone are not helpful to obtain the required displacements and tractions acting on the boundaries of the center unit cell. To derive the

further helpful relations between the deformations on either faces of the center unit cell, the concept of Equivalent Coordinate System (ECS) [14] is employed which is discussed in the next section.

b. Symmetry Relations Using Equivalent Coordinate Systems (ECS)

Consider the free body diagram of the center unit cell shown in Figure 14. Consider a new coordinate system $\bar{x}_i$ obtained by taking the mirror image of the original coordinate system x_i about the plane x_2x_3. Note that the loads acting on the unit cell in the new coordinate system are the same as those in original coordinate system but with a switch in their sign. If the unit cell (both geometry and material distribution) also exhibits a mirror symmetry about x_2x_3 plane, then the new coordinate system acts as the Equivalent Coordinate System for the current problem[9].

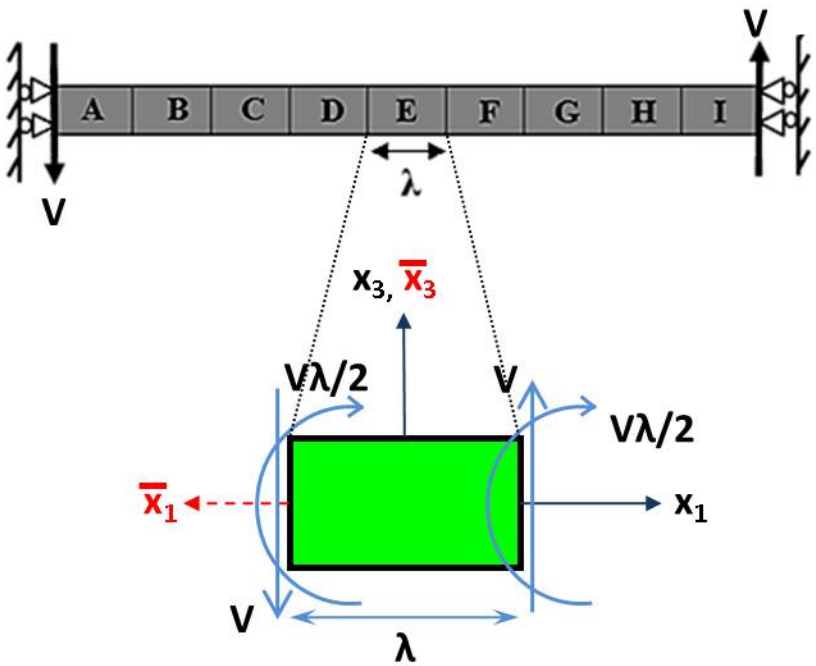

Fig. 14. Equivalent coordinate system for a beam under end shear loads

If $\bar{x}_i = a_{ij}x_j$, then

$$a_{ij} = \begin{bmatrix} -1 & 0 & 0 \\ 0 & 1 & 0 \\ 0 & 0 & 1 \end{bmatrix} \tag{2.33}$$

The field variables in the unit cell corresponding to the original coordinate system can be related to the ones corresponding to the new coordinate sytem as,

$$\begin{aligned} \gamma\bar{u}_i\left(\bar{x}_\alpha\right) &= u_i\left(x_\alpha\right) \\ \gamma\frac{\partial\bar{u}_i}{\partial\bar{x}_j}\left(\bar{x}_\alpha\right) &= \frac{\partial u_i}{\partial x_j}\left(x_\alpha\right) \\ \gamma\bar{\varepsilon}_{ij}\left(\bar{x}_\alpha\right) &= \varepsilon_{ij}\left(x_\alpha\right) \\ \gamma\bar{\sigma}_{ij}\left(\bar{x}_\alpha\right) &= \sigma_{ij}\left(x_\alpha\right) \end{aligned} \tag{2.34}$$

where γ takes a value of -1 because the loads in the new coordinate system are opposite to those in the original coordinate system. Since the new coordinate system $\bar{x}_i$ is related to x_i through a_{ij}, the field variables in $\bar{x}_i$ can be transformed to x_i as follows,

$$\begin{aligned} \bar{u}_i\left(\bar{x}_\alpha\right) &= a_{ij}u_j\left(a_{\alpha k}x_k\right) \\ \frac{\partial\bar{u}_i}{\partial\bar{x}_j}\left(\bar{x}_\alpha\right) &= a_{im}a_{jn}\frac{\partial u_m}{\partial x_n}\left(a_{\alpha k}x_k\right) \\ \bar{\varepsilon}_{ij}\left(\bar{x}_\alpha\right) &= a_{im}a_{jn}\varepsilon_{mn}\left(a_{\alpha k}x_k\right) \\ \bar{\sigma}_{ij}\left(\bar{x}_\alpha\right) &= a_{im}a_{jn}\sigma_{mn}\left(a_{\alpha k}x_k\right) \end{aligned} \tag{2.35}$$

Combining Eqs. (2.34) and (2.35) and using $\bar{x}_i = a_{ij}x_j$ gives,

$$\begin{aligned} u_i\left(x_\alpha\right) &= \gamma a_{ij} u_j\left(a_{\alpha k}x_k\right) \\ \frac{\partial u_i}{\partial x_j}\left(x_\alpha\right) &= \gamma a_{im}a_{jn}\frac{\partial u_m}{\partial x_n}\left(a_{\alpha k}x_k\right) \\ \varepsilon_{ij}\left(x_\alpha\right) &= \gamma a_{im}a_{jn}\varepsilon_{mn}\left(a_{\alpha k}x_k\right) \\ \sigma_{ij}\left(x_\alpha\right) &= \gamma a_{im}a_{jn}\sigma_{mn}\left(a_{\alpha k}x_k\right) \end{aligned} \tag{2.36}$$

Substituting the value of a_{ij} given in Eq. (2.33) into Eq. (2.36) gives the following ECS relations,

$$\begin{aligned} \text{For } i = 1 \;\Rightarrow\; u_1\left(x_1, x_2, x_3\right) &= u_1\left(-x_1, x_2, x_3\right) \\ i = 2, 3 \Rightarrow\; u_i\left(x_1, x_2, x_3\right) &= -u_i\left(-x_1, x_2, x_3\right) \end{aligned} \tag{2.37}$$

$$\begin{aligned} \text{For } i = j = 1, 2, 3 \text{ and } (i, j) = (2, 3) \text{ or } (3, 2) & \\ \frac{\partial u_i}{\partial x_j}\left(x_1, x_2, x_3\right) &= -\frac{\partial u_i}{\partial x_j}\left(-x_1, x_2, x_3\right) \\ \Rightarrow\; \varepsilon_{ij}\left(x_1, x_2, x_3\right) &= -\varepsilon_{ij}\left(-x_1, x_2, x_3\right) \\ \sigma_{ij}\left(x_1, x_2, x_3\right) &= -\sigma_{ij}\left(-x_1, x_2, x_3\right) \end{aligned} \tag{2.38}$$

$$\begin{aligned} \text{For } i \neq j = 1, 2, 3 \text{ and } (i, j) \neq (2, 3) \text{ or } (3, 2) & \\ \frac{\partial u_i}{\partial x_j}\left(x_1, x_2, x_3\right) &= \frac{\partial u_i}{\partial x_j}\left(-x_1, x_2, x_3\right) \\ \Rightarrow\; \varepsilon_{ij}\left(x_1, x_2, x_3\right) &= \varepsilon_{ij}\left(-x_1, x_2, x_3\right) \\ \sigma_{ij}\left(x_1, x_2, x_3\right) &= \sigma_{ij}\left(-x_1, x_2, x_3\right) \end{aligned} \tag{2.39}$$

By substituting $x_1 = -\frac{\lambda}{2}$ in Eqs. (2.34) - (2.39) give relations between the field variables on the end faces of the center unit cell. Using the ECS relations for the displacement gradients at $x_1 = -\frac{\lambda}{2}$ in Eq. (2.31) gives for the cases of $(i, j) =$

$(1,1),(2,2),(3,3)$ and $(2,3)$,

$$\begin{aligned} \frac{\partial u_i}{\partial x_j}\left(\frac{\lambda}{2},x_2,x_3\right) &= -\frac{\partial u_i}{\partial x_j}\left(\frac{\lambda}{2},x_2,x_3\right)+\frac{\partial \hat{u}_i}{\partial x_j}\left(-\frac{\lambda}{2},x_2,x_3\right) \\ \Rightarrow \frac{\partial u_i}{\partial x_j}\left(\frac{\lambda}{2},x_2,x_3\right) &= \frac{1}{2}\frac{\partial \hat{u}_i}{\partial x_j}\left(-\frac{\lambda}{2},x_2,x_3\right)=\frac{1}{2}\frac{\partial \hat{u}_i}{\partial x_j}\left(\frac{\lambda}{2},x_2,x_3\right) \end{aligned} \tag{2.40}$$

Equation (2.40) shows that the displacement gradients on the end faces of the center unit cell are explicitly related to the ones corresponding to the constant moment deformation. The conditions on the gradients $\frac{\partial u_2}{\partial x_2}, \frac{\partial u_3}{\partial x_3}$ and $\frac{\partial u_2}{\partial x_3}$ can be imposed by imposing the in-plane displacements u_2 and u_3 as follows,

$$u_i\left(\pm\frac{\lambda}{2},x_2,x_3\right)=\pm\frac{1}{2}\hat{u}_i\left(\frac{\lambda}{2},x_2,x_3\right)\ \ i=2,3 \tag{2.41}$$

But the conditions on the displacement gradient $\frac{\partial u_1}{\partial x_1}$ cannot imposed just by imposing the conditions on the displacement u_1 at the end faces. Hence a new set of relations are required to get the conditions in the normal (x_1) direction on the end faces of the unit cell. The ECS and superposition relations in displacement gradients for the cases of $(i,j)=(1,2)$ and $(1,3)$ do not give any useful relations.

To derive the BC's in the normal direction on the end faces, we use the superposition and ECS relations stresses. Substituting $x_1=-\frac{\lambda}{2}$ in Eq. (2.32) gives,

$$\sigma_{ij}\left(\frac{\lambda}{2},x_2,x_3\right)=\sigma_{ij}\left(-\frac{\lambda}{2},x_2,x_3\right)+\hat{\sigma}_{ij}\left(-\frac{\lambda}{2},x_2,x_3\right)\ \ i,\ j\ =\ 1,\ 2,\ 3 \tag{2.42}$$

Using the symmetry relations in terms of stresses given in Eqs. (2.37)-(2.39) for $x_1=-\frac{\lambda}{2}$, Eq. (2.42) gives the following relations for the stresses on the end faces,

$$\begin{aligned} \text{For } i\ =\ j:\ \sigma_{ij}\left(\frac{\lambda}{2},x_2,x_3\right) &= -\sigma_{ij}\left(\frac{\lambda}{2},x_2,x_3\right)+\hat{\sigma}_{ij}\left(-\frac{\lambda}{2},x_2,x_3\right) \\ \Rightarrow \sigma_{ij}\left(\frac{\lambda}{2},x_2,x_3\right) &= \frac{1}{2}\hat{\sigma}_{ij}\left(-\frac{\lambda}{2},x_2,x_3\right)=\frac{1}{2}\hat{\sigma}_{ij}\left(\frac{\lambda}{2},x_2,x_3\right) \end{aligned} \tag{2.43}$$

Considering the case of $i = j = 1$, Eq. (2.43) gives,

$$\sigma_{11}\left(\frac{\lambda}{2}, x_2, x_3\right) = \frac{1}{2}\hat{\sigma}_{11}\left(\frac{\lambda}{2}, x_2, x_3\right) \tag{2.44}$$

Using Cauchy's formula, $T_i = \sigma_{ji} n_j$, the relation in stresses given by Eq. (2.44) can be converted to a relation in tractions. Here n_j represent the components of the normal the surface. For the end faces of the unit cell $n_j = (\pm 1, 0, 0)$. So, the tractions in the normal direction in terms of stresses on the end faces of the unit cell are given by,

$$T_1\left(\pm\frac{\lambda}{2}, x_2, x_3\right) = \pm\sigma_{11}\left(\pm\frac{\lambda}{2}, x_2, x_3\right) \tag{2.45}$$

Combining Eqs. (2.44) and (2.45) gives the following conditions on tractions in the normal direction for the center unit cell,

$$T_1\left(\pm\frac{\lambda}{2}, x_2, x_3\right) = \frac{1}{2}\hat{T}_1\left(\frac{\lambda}{2}, x_2, x_3\right) \tag{2.46}$$

In summary, by combining Eqs. (2.41) and (2.46), the BC's for the shear mode can be written as,

$$\begin{aligned} T_1\left(\pm\frac{\lambda}{2}, x_2, x_3\right) &= \frac{1}{2}\hat{T}_1\left(\frac{\lambda}{2}, x_2, x_3\right) \\ u_i\left(\pm\frac{\lambda}{2}, x_2, x_3\right) &= \pm\frac{1}{2}\hat{u}_i\left(\frac{\lambda}{2}, x_2, x_3\right) \;\; i = 2, 3 \end{aligned} \tag{2.47}$$

Note that Eq. (2.47) gives BCs for both the shear modes. If the terms $\hat{T}_1$ and $\hat{u}_j$ correspond to a constant incremental moment about x_3 (ΔM_3), then the BC's in Eq. (2.47) correspond to the shear along x_2 (F_2) and if they correspond to a constant incremental moment about x_2 (ΔM_2) then the BC's in Eq. (2.47) correspond to the shear along x_3 (F_3). The solution for the constant moment part in Eq. (2.47) can be obtained using the boundary conditions derived in the previous section i.e. using Eqs. (2.28) and (2.29). Figure 15 shows the results obtained for the beam shown in

Figure 11 using the correct BC's given in Eq. (2.47). The figure illustrates that the shear stress contours in the unit cell are uniform along the length showing no end effects.

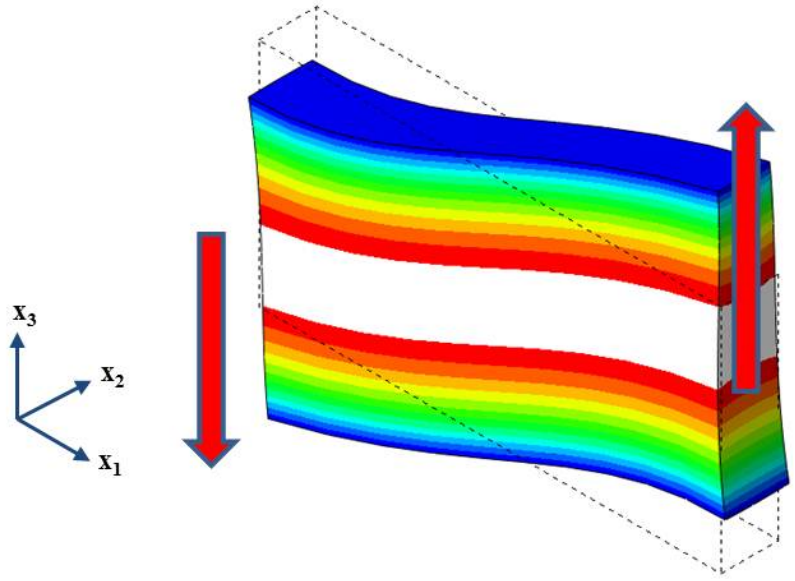

Fig. 15. Shear deformation of the unit cell using the correct BC's derived from the superposition method

Equations (2.26)-(2.29) and (2.47) give the complete set of BCs for the six fundamental modes. Note that the rigid body constraints are not specified in these BC's since they depend on the particular configuration being analyzed. 3D FEA is employed to evaluate the corresponding deformations and strain energies. Formulation of the 3D FEA is derived in the next chapter.

G. Translation of the Beam Reference Axis and the Prediction of Centroid and Shear Center Locations

The effective properties predicted from the homogenization method described in the previous section depend on the location of the reference axis in the coordinate system.

This is because the definitions of beam stress resultants (R_i in Eq. (2.12) and the generalized strains (e_i in Eqs. (2.10) and (2.16)) depend on the location of the coordinate system. For the beam analysis, the x_1 axis with respect to which the effective properties are obtained, acts as the beam reference axis. If the effective properties with respect to one coordinate system are known, then they can be transformed to obtain the properties in a new coordinate system located at a different location in the cross section. This can be accomplished by using the transformation matrices that transform R_i and e_i.

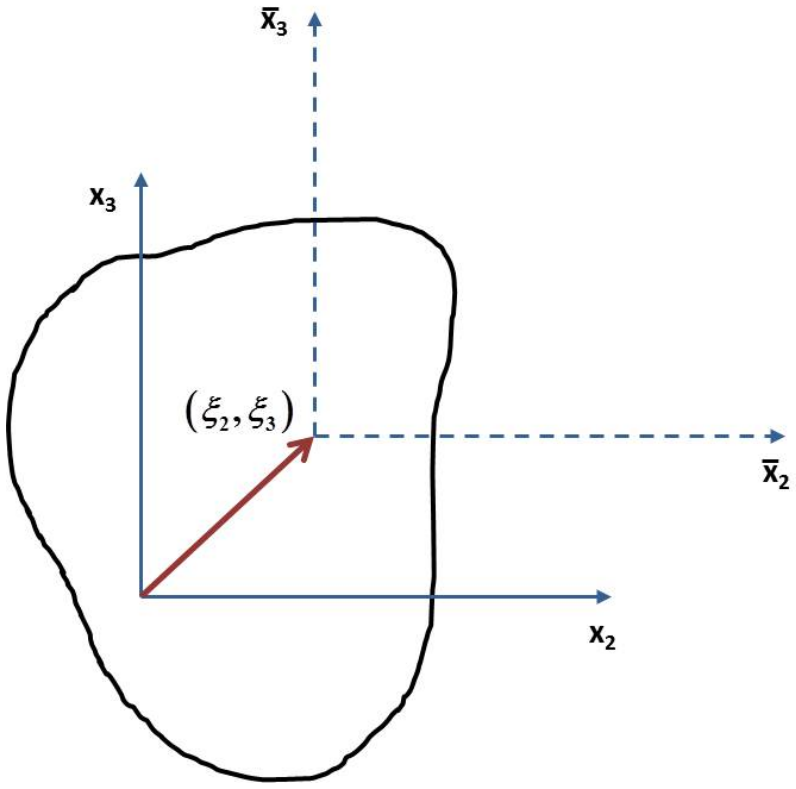

Fig. 16. Schematic showing the translation of reference axis in the cross section

Consider the arbitrary cross section with the two coordinate systems x_i and $\bar{x}_i$ shown in Figure 16. Let the origin of the coordinate system $\bar{x}_i$ (referred to as new coordinate system in the following discussion) be located at $(0, \xi_2, \xi_3)$ with respect

to the coordinate system x_i. Note that the resultants in each coordinate system are defined relative to the location of the corresponding reference axis in the cross section. Hence the resultants R_i in the coordinate system x_i are related to the resultants $\bar{R}_i$ in the new coordinate system $\bar{x}_i$ as follows,

$$\begin{aligned} R_i &= T_{ij}\bar{R}_j \\ \text{where } T &= \begin{bmatrix} 1 & 0 & 0 & 0 & 0 & 0 \\ 0 & 1 & 0 & 0 & 0 & 0 \\ 0 & 0 & 1 & 0 & 0 & 0 \\ 0 & -\xi_3 & \xi_2 & 1 & 0 & 0 \\ \xi_3 & 0 & 0 & 0 & 1 & 0 \\ -\xi_2 & 0 & 0 & 0 & 0 & 1 \end{bmatrix} \end{aligned} \tag{2.48}$$

Similarly, the generalized strain e_i and $\bar{e_i}$ are related as follows,

$$e_i = T_{ij}^{-T}\bar{e_j} \tag{2.49}$$

Using the Eqs. (2.14), (2.48) and (2.49), the relation between $\bar{R}_i$ and the strains $\bar{e_i}$ can be obtained as,

$$\begin{aligned} \bar{R}_i &= \bar{C}_{ij}\bar{e}_j \\ \text{where } \bar{C}_{ij} &= {T_{ij}}^{-1} C_{jk} {T_{lk}}^{-1} \end{aligned} \tag{2.50}$$

Hence the transformation matrix for the effective stiffness matrix is given by $\mathbf{T^{-1}CT^{-T}}$ where $\mathbf{T}$ is given by Eq. (2.48). The relation for the transformed stiffness matrix given in Eq. (2.50) can be used to predict the locations of weighted centroid and shear center of the cross section. The weighted centroid and shear centers are characteristic locations in each cross section of a slender member. The prediction of these locations helps simplify the aeroelastic analyses of complex slender members like wind turbine blades to a great extent.

The weighted centroid of a cross section is defined as the point at which the resultant axial force (F_1) should act under a pure extension (i.e. e_1 = constant and rest all e_i are zero) such that there are no resultant moments generated in the cross section. In other words, if the reference axis is located at the weighted centroid of the cross section, the extension-flexure coupling terms C_{15} and C_{16} in the corresponding stiffness matrix should be zero. Suppose that the weighted centroid of a cross section is located at (ξ_{2c}, ξ_{3c}) with respect to x_i. If C_{ij} is the stiffness matrix in x_i and $\bar{C_{ij}}$ is the stiffness matrix in the coordinate system placed at weighted centroid $((\xi_{2c}, \xi_{3c}))$, then the terms $\bar{C_{12}}$ and $\bar{C_{13}}$ should be zero. Since these terms will be functions of (ξ_{2c} and ξ_{3c}) from the relation given Eq. (2.50), the coordinates of the weighted centroid can be found as given below,

$$\begin{aligned} \xi_{2c} &= -\frac{C_{16}}{C_{11}} \\ \xi_{3c} &= \frac{C_{15}}{C_{11}} \end{aligned} \tag{2.51}$$

The shear center of cross section is defined as the point at which the resultant shear forces (F_2 and F_3) should act such that there is no torque generated in the cross section (assuming no external torque is applied on the beam). In other words, if the reference axis is located at the shear center, the shear-torsion coupling terms C_{24} and C_{34} in the corresponding stiffness matrix should be zero. Following the same procedure as described for finding the weighted centroid, the coordinates of the shear center (ξ_{2sc} and ξ_{3sc}) can be found as given below,

$$\begin{aligned} \xi_{2sc} &= \frac{C_{22}C_{34} - C_{23}C_{24}}{C_{22}C_{33} - {C_{23}}^2} \\ \xi_{3sc} &= \frac{C_{23}C_{34} - C_{24}C_{33}}{C_{22}C_{33} - {C_{23}}^2} \end{aligned} \tag{2.52}$$

The Eqs. (2.51) and (2.52) provide a quick and accurate way of predicting the centroid and shear center locations once the effective stiffness matrix is predicted

corresponding to at least one location of the reference axis.

CHAPTER III

FINITE ELEMENT FORMULATIONS

In the previous chapter, BC's are derived for analysis using the Quasi-3D (Q3D) and Unit Cell methods. It is not possible in general to obtain the closed form solutions for the deformations in the beam using these BC's. Hence numerical techniques are required to predict approximate solutions. In this chapter, detailed formulations are derived for the finite element method based on linear elasticity. Note that the Unit Cell method requires a 3D domain (unit cell) to be analyzed whereas the Q3D method requires a 2D domain (cross section) of the slender member needs to analyzed. Also the governing equations for the Generalized Euler-Bernoulli and Generalized-Timoshenko beam theories require a 1D finite element formulation for the beam analysis. First the weak form of governing equations are developed based on the approach discussed in [15]. Then the concept of finite element discretization are employed for solving the governing equations for 3D elasticity, the Q3D analysis and the beam analysis.

A. Weak Form for 3D Elasticity

The problem statement as presented for 3D elasticity in the previous chapter is referred to as the "strong form". A "weak form" statement of the same problem represents an integral statement which can be obtained by multiplying the equilibrium equations in Eq. (2.1) with virtual displacements, δu_i and integrating them over the domain of the problem Ω.

$$\int_{\Omega} \delta u_i \left(\frac{\partial \sigma_{ij}}{\partial x_j} + f_i \right) d\Omega = 0 \tag{3.1}$$

The derivatives on stresses in Eq. (3.1) can be transfered on to the virtual displacements by using integration by parts.

$$\oint_{\Gamma} \sigma_{ij}\delta u_i n_j d\Gamma - \int_{\Omega} \sigma_{ij}\frac{\partial \delta u_i}{\partial x_j} d\Omega + \int_{\Omega} f_i \delta u_i d\Omega = 0 \tag{3.2}$$

Using Eq. (2.1b) and Eq. (2.3),

$$\oint_{\Gamma} \sigma_{ji} n_j \delta u_i d\Gamma - \int_{\Omega} \sigma_{ij}\left(\frac{\partial \delta u_i}{\partial x_j} + \frac{\partial \delta u_j}{\partial x_i}\right) d\Omega + \int_{\Omega} f_i \delta u_i d\Omega = 0 \tag{3.3}$$

Using the Cauchy's formula, $T_i = \sigma_{ji} n_j$,

$$\oint_{\Gamma} T_i \delta u_i d\Gamma - \int_{\Omega} \sigma_{ij}\delta \varepsilon_{ij} d\Omega + \int_{\Omega} f_i \delta u_i d\Omega = 0 \tag{3.4}$$

The stresses σ_{ij} can be written in terms of strains using the constitutive relations given in Eq. (2.2),

$$\oint_{\Gamma} T_i \delta u_i d\Gamma - \int_{\Omega} C_{ijkl}\varepsilon_{kl}\delta \varepsilon_{ij} d\Omega + \int_{\Omega} f_i \delta u_i d\Omega = 0 \tag{3.5}$$

Equation (3.5) along with BC's given by Eq. (2.4) constitute the complete problem statement in weak form for linear elasticity. Exact analytical solutions can be found using either the strong form or the weak form for simple problems. But if the complexity of the problem increases, it becomes impossible to obtain the exact solutions. In such cases, the weak form can be used to find approximate solutions. If the virtual displacements δu_i are chosen to take some form of a series of analytical functions (known as approximation functions or shape functions) with unknown coefficients, the integral statement can be reduced to a system of algebraic equations. Solving these equations for the unknown coefficients, an approximate solution for the problem can be obtained. However the set of approximation functions need to satisfy the following set of conditions to give a valid solution:

1. They must be sufficiently differentiable and integrable to evaluate the integrals in the weak form.

2. The set of functions must be linearly independent.

This approach of obtaining the solutions from the weak form of the partial differential equations is known as the variational method. It is in general difficult to find the set of approximation functions over the whole domain Ω of the problem. The finite element analysis technique presents a systematic way of constructing these functions which is discussed in the following section.

B. 3D Finite Element Analysis

Finite element analysis (FEA) is a method of obtaining approximate solutions using the weak form of the partial differential equations. In 3D linear elasticity, the finite element method discretizes the actual domain of the problem into sub domains called elements and considers the weak form as a sum of integrals over each sub domain Ω_e given by,

$$\sum_{e=1}^{N} \left(\oint_{\Gamma_e} T_i \delta u_i d\Gamma_e - \int_{\Omega_e} C_{ijkl} \varepsilon_{kl} \delta \varepsilon_{ij} d\Omega_e + \int_{\Omega_e} f_i \delta u_i d\Omega_e \right) = 0 \tag{3.6}$$

The integrals over each element give a sub-system of algebraic equations. These element level equations are then assembled in to a global system of equations by enforcing the continuity and equilibrium conditions at element boundaries. This process is called as the "Assembly" process in FEA.

First the element level equations need to be obtained. An analytical form in terms of approximation functions is assumed for the displacements in each element as follows,

$$u_i = u_i^k \psi_k \qquad on \qquad \Omega_e \tag{3.7}$$

where u_i^k are the unknown coefficients and ψ_k are the known analytical functions called shape functions. The unknown coefficients u_i^k can be written in a vector form as follows,

$$q_\beta = \left\{ \begin{array}{ccc|ccc|c|ccc} u_1^1 & u_2^1 & u_3^1 & u_1^2 & u_2^2 & u_3^2 & ... & u_1^n & u_2^n & u_3^n \end{array} \right\} \tag{3.8}$$

The variation of the displacements and strains can now be written as,

$$\begin{aligned} \delta u_i &= \frac{\partial u_i}{\partial q_\beta} \delta q_\beta \\ \delta \varepsilon_{ij} &= \frac{\partial \varepsilon_{ij}}{\partial q_\beta} \delta q_\beta \end{aligned} \tag{3.9}$$

Substituting the above notations in the Eq. (3.6) and taking the virtual unknown coefficients δq_β as common factor from all terms gives,

$$\sum_{e=1}^{N} \left(\oint_{\Gamma_e} T_i \frac{\partial u_i}{\partial q_\beta} d\Gamma_e - \int_{\Omega_e} C_{ijkl} \frac{\partial \varepsilon_{kl}}{\partial q_\rho} \frac{\partial \varepsilon_{ij}}{\partial q_\beta} q_\rho d\Omega_e + \int_{\Omega_e} f_i \frac{\partial u_i}{\partial q_\beta} d\Omega_e \right) \delta q_\beta = 0 \tag{3.10}$$

The Eq. (3.10) should be satisfied for any arbitrary values of δq_β. Hence the terms in the parenthesis must be zero over Ω_e.

$$\oint_{\Gamma_e} T_i \frac{\partial u_i}{\partial q_\beta} d\Gamma_e - \int_{\Omega_e} C_{ijkl} \frac{\partial \varepsilon_{kl}}{\partial q_\beta} \frac{\partial \varepsilon_{ij}}{\partial q_\beta} q_\rho d\Omega_e + \int_{\Omega_e} f_i \frac{\partial u_i}{\partial q_\beta} d\Omega_e = 0 \tag{3.11}$$

To derive the system of linear equations, it is convenient to adopt Voigt notation for the tensors in Eq. (3.6). Voigt notation can be obtained by replacing the tensorial indices with the new indices i.e. by replacing $11, 22, 33, 23, 13, 12$ with $1, 2, 3, 4, 5, 6$ respectively. Also the strains ϵ_i (Voigt notation) can be conveniently written in the following form.

$$\varepsilon_\alpha = B_{\alpha\beta} q_\beta \tag{3.12}$$

where,

$$B_{\alpha\beta} = \frac{\partial \varepsilon_\alpha}{\partial q_\beta} = \left[\begin{array}{ccc|c|ccc} \frac{\partial \psi_1}{\partial x_1} & 0 & 0 & & \frac{\partial \psi_n}{\partial x_1} & 0 & 0 \\ 0 & \frac{\partial \psi_1}{\partial x_2} & 0 & & 0 & \frac{\partial \psi_n}{\partial x_2} & 0 \\ 0 & 0 & \frac{\partial \psi_1}{\partial x_3} & ..... & 0 & 0 & \frac{\partial \psi_n}{\partial x_3} \\ 0 & \frac{\partial \psi_1}{\partial x_3} & \frac{\partial \psi_1}{\partial x_2} & & 0 & \frac{\partial \psi_n}{\partial x_3} & \frac{\partial \psi_n}{\partial x_2} \\ \frac{\partial \psi_1}{\partial x_3} & 0 & \frac{\partial \psi_1}{\partial x_1} & & \frac{\partial \psi_n}{\partial x_3} & 0 & \frac{\partial \psi_n}{\partial x_1} \\ \frac{\partial \psi_1}{\partial x_2} & \frac{\partial \psi_1}{\partial x_1} & 0 & & \frac{\partial \psi_n}{\partial x_2} & \frac{\partial \psi_n}{\partial x_1} & 0 \end{array}\right] \tag{3.13}$$

Also the gradients of displacements in Eq. (3.11) can be written in terms of the shape functions as follows,

$$\frac{\partial u_i}{\partial q_\beta} = \left[\begin{array}{ccc|ccc|c|ccc} \psi_1 & 0 & 0 & \psi_2 & 0 & 0 & & \psi_n & 0 & 0 \\ 0 & \psi_1 & 0 & 0 & \psi_2 & 0 & ... & 0 & \psi_n & 0 \\ 0 & 0 & \psi_1 & 0 & 0 & \psi_2 & & 0 & 0 & \psi_n \end{array}\right] \tag{3.14}$$

Substituting Eqs. (3.12) and (3.14) in to Eq. (3.11) gives the following algebraic equations,

$$\begin{aligned} K^e_{\beta\rho} q_\rho &= F^e_\beta \\ \text{where } K^e_{\beta\rho} &= \int_{\Omega_e} C_{\alpha\gamma} B_{\gamma\beta} B_{\alpha\beta} d\Omega_e \\ F^e_\beta &= \oint_{\Gamma_e} T_i \frac{\partial u_i}{\partial q_\beta} d\Gamma_e + \int_{\Omega_e} f_i \frac{\partial u_i}{\partial q_\beta} d\Omega_e \end{aligned} \tag{3.15}$$

The integrals in the element level matrices (K^e_{ij} and F^e_i can be evaluated using numerical integration schemes. Any numerical integration scheme evaluates definite integrals (exactly or approximately depending on the order of the integrand) as a weighted sum of values of the functions at finite number of points, called "integration" points, in the domain of the integral. The Gauss-Legendre numerical integration

scheme evaluates the integrals as shown below,

$$\int_{-1}^{1} g\left(x\right)dx = \sum_{i=1}^{n_{gp}} g\left(x_i\right) W_i \qquad i = 1..n_{gp} \tag{3.16}$$

where $G(x)$ is the integrand, x_i are integration points and W_i are the weights. The Gauss-Lengendre scheme gives a set of integration points and the corresponding weights over the domain $(-1, 1)$ which are shown in Table I. The 1D integral in Eq. (3.16) can be extended to 3D to evaluate the element matrices given in Eq. (**??**). The master domain for the 3D integration will be a cube ranging from -1 to 1 along the three coordinate axes with its center at origin (see Figure 17).

Table I. Integration points and their weights for Gauss-Legendre numerical integration

n_{gp}	ξ_i	w_i
1	0	2
2	$\pm\sqrt{\frac{1}{3}}$	1,1
3	0,$\pm\sqrt{\frac{1}{3}}$	$\frac{8}{9},\frac{5}{9},\frac{5}{9}$

To evaluate the integrals in the element matrices, since the integration points and the weights are defined over the master domain shown in Figure 17, the geometry of all elements need to be spatially mapped to the master domain. The geometry of the element domain can be mapped to the master domain as follows,

$$x_i = x_i^k \hat{\psi}_k \left(\xi_1, \xi_2, \xi_3\right) \qquad k = 1 \ldots m \tag{3.17}$$

where x_i^k are the coordinates of some finite number of points in the element domain. These points are referred to as "nodes" in FEA. The functions $\hat{\psi}_k$ in the Eq. (3.17) can be any arbitrary analytical functions. If $\hat{\psi}_k$ and ψ_k are chosen to be the same set of functions, then the element under consideration is termed as Isoparametric. Isoparametric elements are used for all the models analyzed in the current work the

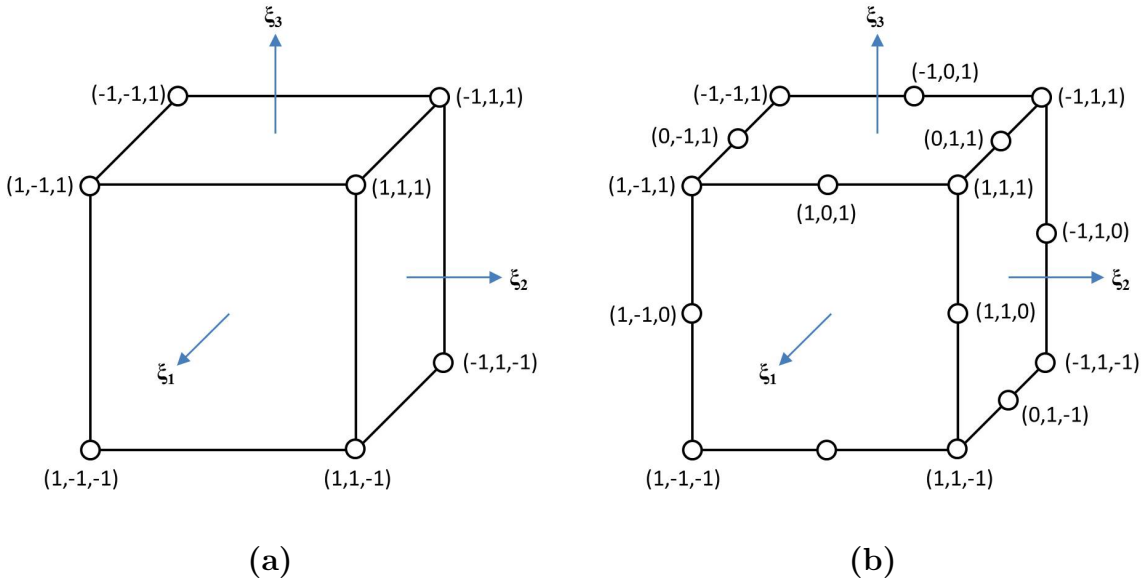

Fig. 17. 3D master elements **(a)** 8-Noded **(b)** 20-Noded

following discussion also correspond to the same.

The Jacobian of the transformation given in Eq. (3.17) is,

$$J_{ij} = \frac{\partial x_j}{\partial \xi_i} = x_j^k \frac{\partial \hat{\psi}_k}{\partial \xi_i} \tag{3.18}$$

This implies the derivatives of shape functions with respect to the actual coordinates x_i can be written in terms of the derivatives in master element coordinates ξ_i as,

$$\frac{\partial \psi_k}{\partial x_j} = \frac{\partial \psi_k}{\partial \xi_i}\frac{\partial \xi_i}{\partial x_j} = J_{ij}^{-1}\frac{\partial \psi_k}{\partial \xi_i} \tag{3.19}$$

Substituting Eq. (3.19) into Eq. (3.15) gives,

$$\begin{aligned} & K^e_{\beta\rho} q_\rho = F^e_\beta \\ & \text{where} \qquad K^e_{\beta\rho} = \int\limits_{\Omega_{\xi e}} \left(C_{\alpha\gamma} B_{\gamma\beta} B_{\alpha\beta}\right) |J| \, d\Omega_{\xi e} \\ & \qquad\qquad F^e_\beta = \int\limits_{\Omega_{\xi e}} \left(f_i \frac{\partial u_i}{\partial q_\beta}\right) |J| \, d\Omega_{\xi e} + \oint\limits_{\Gamma_{\xi e}} \left(T_i \frac{\partial u_i}{\partial q_\beta}\right) |J| \, d\Gamma_{\xi e} \end{aligned} \tag{3.20}$$

Using the Guass-Legendre integration scheme, the element matrices can be written

as,

$$\begin{aligned} K^e_{\beta\rho} &= \sum_{k=1}^{n_{gp}} \left(C_{\alpha\gamma} B_{\gamma\beta} B_{\alpha\beta}\right)\big|_{\xi^k} |J|\, w_1^k w_2^k w_3^k \\ F^e_{\beta} &= \sum_{k=1}^{n_{gp}} \left(f_i \tfrac{\partial u_i}{\partial q_\beta}\right)\Big|_{\xi^k} |J|\, w_1^k w_2^k w_3^k + \oint\limits_{\Gamma_{\xi e}} \left(T_i \tfrac{\partial u_i}{\partial q_\beta}\right) |J|\, d\Gamma_{\xi e} \end{aligned} \tag{3.21}$$

where n_{gp} represents the number of integration points in the element.

Note that the above relations are derived for any set of shape functions which satisfy the requirements mentioned previously. Regular polynomial functions can be considered as shape functions but the unknown coefficients u_i^k in such a case do not possess any direct physical meaning. This makes the assembly process to be tedious especially if there large number of elements in the domain. For a systematic assembly process the shape functions are defined such that the unknown coefficients u_i^k represent the displacement values at certain points in or on the boundary of the element. These points are termed as "nodes" of that particular element. Equation (3.7) indicates that the number of shape functions corresponding to each displacement component u_i for a given element is equal to the number of unknown coefficients u_i^k. Hence if the unknown coefficients represent the displacement values at nodes, the number of shape functions should be equal to the number of nodes in the element. The shape functions for 8-noded and 20-noded brick elements shown in Figure 17 are derived in the next section.

C. Shape Functions for Brick Elements

For 8-noded brick elements the displacement can at most vary in the form of a least order polynomial of 8 terms.

$$\begin{aligned} u_i\left(\xi_1, \xi_2, \xi_3\right) = a_1^i + a_2^i \xi_1 + a_3^i \xi_2 + a_4^i \xi_3 + a_5^i \xi_1 \xi_2 + a_6^i \xi_2 \xi_3 \\ + a_7^i \xi_3 \xi_1 + a_8^i \xi_1 \xi_2 \xi_3 \end{aligned} \tag{3.22}$$

Equation (3.30) can be conveniently written in the following,

$$\begin{aligned} u_i(\xi_1,\xi_2,\xi_3) &= X_j^i(\xi_1,\xi_2,\xi_3)\,A_j^i \\ \text{where } X_j^i &= \left\{ \begin{array}{cccccccc} 1 & \xi_1 & \xi_2 & \xi_3 & \xi_1\xi_2 & \xi_2\xi_3 & \xi_3\xi_1 & \xi_1\xi_2\xi_3 \end{array} \right\} \\ A_j^i &= \left\{ \begin{array}{cccccccc} a_1^i & a_2^i & a_3^i & a_4^i & a_5^i & a_6^i & a_7^i & a_8^i \end{array} \right\}^T \end{aligned} \tag{3.23}$$

Since the unknown coefficients u_i^k in Eq. (3.7) are the nodal displacement values,

$$u_i^k = u_i\left(\xi_1^k,\xi_2^k,\xi_3^k\right) = X_j^i\left(\xi_1^k,\xi_2^k,\xi_3^k\right)A_j^i \tag{3.24}$$

where ξ_i^k represent the nodal coordinates. Equation (3.24) can be written in the matrix form as,

$$\begin{aligned} &\Delta_k^i = G_{kj}^i A_j^i \\ &\text{where } \Delta_k^i = \left\{ \begin{array}{c} u_i^1 \\ \vdots \\ u_i^k \\ \vdots \\ u_i^n \end{array} \right\} \text{ and } G_{kj}^i = \left[\begin{array}{c} X_j^i\left(\xi_1^1,\xi_2^1,\xi_3^1\right) \\ \vdots \\ X_j^i\left(\xi_1^k,\xi_2^k,\xi_3^k\right) \\ \vdots \\ X_j^i\left(\xi_1^n,\xi_2^n,\xi_3^n\right) \end{array} \right] \end{aligned} \tag{3.25}$$

The polynomial coefficient matrix A_j^i can now be written in terms of the nodal displacements as,

$$A_j^i = \left(G_{kj}^i\right)^{-1}\Delta_k^i \tag{3.26}$$

Substituting Eq. (3.26) into Eq. (3.23) gives,

$$u_i = X_j^i\left(G_{kj}^i\right)^{-1}\Delta_k^i \tag{3.27}$$

Hence the shape functions are given by the following matrix form,

$$\Psi = XG^{-1} \tag{3.28}$$

Evaluating Eq. (3.28) for the 8-noded brick element gives the following set of shape functions.

$$\Psi = \frac{1}{8}\begin{Bmatrix} (1-\xi_1)(1-\xi_2)(1-\xi_3) \\ (1+\xi_1)(1-\xi_2)(1-\xi_3) \\ (1+\xi_1)(1+\xi_2)(1-\xi_3) \\ (1-\xi_1)(1+\xi_2)(1-\xi_3) \\ (1-\xi_1)(1-\xi_2)(1+\xi_3) \\ (1+\xi_1)(1-\xi_2)(1+\xi_3) \\ (1+\xi_1)(1+\xi_2)(1+\xi_3) \\ (1-\xi_1)(1+\xi_2)(1+\xi_3) \end{Bmatrix} \tag{3.29}$$

To derive the shape functions for a 20-noded brick element, assume that the displacements to vary according to the lowest order polynomial of 20 terms given by,

$$\begin{aligned} u_i(\xi_1,\xi_2,\xi_3) = {} & a_1^i + a_2^i\xi_1 + a_3^i\xi_2 + a_4^i\xi_3 + a_5^i\xi_1\xi_2 + a_6^i\xi_2\xi_3 \\ & + a_7^i\xi_3\xi_1 + a_8^i\xi_1\xi_2\xi_3 + a_9^i{\xi_1}^2\xi_2 + a_{10}^i{\xi_2}^2\xi_1 \\ & + a_{11}^i{\xi_2}^2\xi_3 + a_{12}^i{\xi_2}^2\xi_3 + a_{13}^i{\xi_3}^2\xi_1 + a_{14}^i{\xi_1}^2\xi_3 \\ & + a_{15}^i{\xi_1}^2\xi_2\xi_3 + a_{16}^i{\xi_2}^2\xi_3\xi_1 + a_{17}^i{\xi_3}^2\xi_1\xi_2 \\ & + a_{18}^i{\xi_1}^2{\xi_2}^2\xi_3 + a_{19}^i{\xi_2}^2{\xi_3}^2\xi_1 + a_{20}^i{\xi_3}^2{\xi_1}^2\xi_2 \end{aligned} \tag{3.30}$$

By following the same approach as described for 8-noded element, the shape functions

for the 20-noded element can be found as,

$$\Psi = \frac{1}{8}\begin{Bmatrix} (1-\xi_1)(1-\xi_2)(1-\xi_3)(-\xi_1-\xi_2-\xi_3-2) \\ (1+\xi_1)(1-\xi_2)(1-\xi_3)(\xi_1-\xi_2-\xi_3-2) \\ (1+\xi_1)(1+\xi_2)(1-\xi_3)(\xi_1+\xi_2-\xi_3-2) \\ (1-\xi_1)(1+\xi_2)(1-\xi_3)(-\xi_1+\xi_2-\xi_3-2) \\ (1-\xi_1)(1-\xi_2)(1+\xi_3)(-\xi_1-\xi_2+\xi_3-2) \\ (1+\xi_1)(1-\xi_2)(1+\xi_3)(\xi_1-\xi_2+\xi_3-2) \\ (1+\xi_1)(1+\xi_2)(1+\xi_3)(\xi_1+\xi_2+\xi_3-2) \\ (1-\xi_1)(1+\xi_2)(1+\xi_3)(-\xi_1+\xi_2+\xi_3-2) \\ 2\left(1-{\xi_1}^2\right)(1-\xi_2)(1-\xi_3) \\ 2(1+\xi_1)\left(1-{\xi_2}^2\right)(1-\xi_3) \\ 2\left(1-{\xi_1}^2\right)(1+\xi_2)(1-\xi_3) \\ 2(1-\xi_1)\left(1-{\xi_2}^2\right)(1-\xi_3) \\ 2(1-\xi_1)(1-\xi_2)\left(1-{\xi_3}^2\right) \\ 2(1+\xi_1)(1-\xi_2)\left(1-{\xi_3}^2\right) \\ 2(1+\xi_1)(1+\xi_2)\left(1-{\xi_3}^2\right) \\ 2(1-\xi_1)(1+\xi_2)\left(1-{\xi_3}^2\right) \\ 2\left(1-{\xi_1}^2\right)(1-\xi_2)(1+\xi_3) \\ 2(1+\xi_1)\left(1-{\xi_2}^2\right)(1+\xi_3) \\ 2\left(1-{\xi_1}^2\right)(1+\xi_2)(1+\xi_3) \\ 2(1-\xi_1)\left(1-{\xi_2}^2\right)(1+\xi_3) \end{Bmatrix} \tag{3.31}$$

D. Quasi-3D Finite Element Formulation

The deformation in the Quasi-3D (Q3D) behavior does not vary along the axial coordinate x_1 of beams. The deformation only varies within the cross section i.e.

in the x_2x_3 plane. Hence Q3D can be considered as a special case of the 3D linear elasticity. The integrands in Eq. (3.6) for Q3D behavior do not vary along x_1. Hence the integral results in,

$$\left(\oint_{\Gamma_e} T_i \delta u_i d\Gamma_e - \int_{\Omega_e} C_{ijkl}\varepsilon_{kl}\delta\varepsilon_{ij} d\Omega_e + \int_{\Omega_e} f_i \delta u_i d\Omega_e \right) L = 0 \tag{3.32}$$

Since the length of the beam L is a constant the Eq. (3.32) gives,

$$\oint_{\Gamma_e} T_i \delta u_i d\Gamma_e - \int_{\Omega_e} C_{ijkl}\varepsilon_{kl}\delta\varepsilon_{ij} d\Omega_e + \int_{\Omega_e} f_i \delta u_i d\Omega_e = 0 \tag{3.33}$$

Note that the domain of the element Ω_e is 2D. To derive the matrix form for the finite element analysis, let the Q3D displacements given in Eq. (2.24) be written in the following form,

$$\begin{aligned}
u = \Psi q &= \left[\begin{array}{cc} \Psi & \Psi^G \end{array} \right] \left\{ \begin{array}{c} q \\ q^G \end{array} \right\} \\
\text{where } \Psi &= \left[\begin{array}{ccc|ccc|c|ccc} \psi_1 & 0 & 0 & \psi_2 & 0 & 0 & & \psi_n & 0 & 0 \\ 0 & \psi_1 & 0 & 0 & \psi_2 & 0 & \cdots & 0 & \psi_n & 0 \\ 0 & 0 & \psi_1 & 0 & 0 & \psi_2 & & 0 & 0 & \psi_n \end{array} \right] \\
\Psi^G &= \left[\begin{array}{cccc} x_1 & 0 & x_1x_3 & -x_1x_2 \\ 0 & -x_1x_3 & 0 & \frac{1}{2}x_1^2 \\ 0 & x_1x_2 & -\frac{1}{2}x_1^2 & 0 \end{array} \right] \\
q &= \left\{ \begin{array}{ccc|ccc|c|ccc} U_1^1 & U_2^1 & U_3^1 & U_1^2 & U_2^2 & U_3^2 & \cdots & U_1^n & U_2^n & U_3^n \end{array} \right\}^T \\
q^G &= \left\{ \begin{array}{cccc} \varepsilon_1 & \kappa_1 & \kappa_2 & \kappa_3 \end{array} \right\}
\end{aligned} \tag{3.34}$$

The terms with "G" as the superscript correspond to the global modes i.e. extension, torsion and two flexures. Here, Ψ are the shape functions for the variation of the displacements in the cross section plane and hence are functions of x_2 and x_3 only. The

elements level matrices can be obtained by following the same approach as described in the previous section for 3D elasticity. The B matrix in Eq. (3.21) for Q3D deformation looks like,

$$B = \left[\begin{array}{ccc|c|ccc|cccc} 0 & 0 & 0 & & 0 & 0 & 0 & 1 & 0 & x_3 & -x_2 \\ 0 & \frac{\partial \psi_1}{\partial x_2} & 0 & & 0 & \frac{\partial \psi_n}{\partial x_2} & 0 & 0 & 0 & 0 & 0 \\ 0 & 0 & \frac{\partial \psi_1}{\partial x_3} & ..... & 0 & 0 & \frac{\partial \psi_n}{\partial x_3} & 0 & 0 & 0 & 0 \\ 0 & \frac{\partial \psi_1}{\partial x_3} & \frac{\partial \psi_1}{\partial x_2} & & 0 & \frac{\partial \psi_n}{\partial x_3} & \frac{\partial \psi_n}{\partial x_2} & 0 & 0 & 0 & 0 \\ \frac{\partial \psi_1}{\partial x_3} & 0 & 0 & & \frac{\partial \psi_n}{\partial x_3} & 0 & 0 & 0 & x_2 & 0 & 0 \\ \frac{\partial \psi_1}{\partial x_2} & 0 & 0 & & \frac{\partial \psi_n}{\partial x_2} & 0 & 0 & 0 & -x_3 & 0 & 0 \end{array}\right] \tag{3.35}$$

The Gauss-Legendre integration scheme corresponding to a 2D domain is employed to evaluate the integrals present in the element stiffness matrices. The shape functions for the 4-noded and 8-noded 2D master elements are shown in Figure 18 are derived similar to the 3D shape functions.

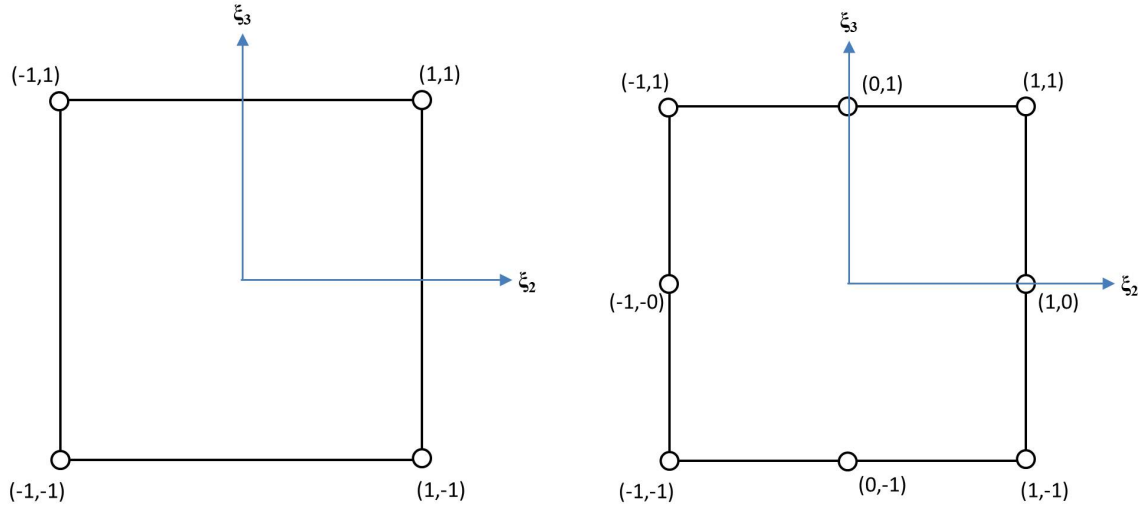

Fig. 18. 2D master elements **(a)** 4-Noded **(b)** 8-Noded

The shape functions corresponding to 4-noded 2D element are given by,

$$\Psi^{2D} = \begin{Bmatrix} \frac{1}{4}(1-\xi_2)(1-\xi_3) \\ \frac{1}{4}(1+\xi_2)(1-\xi_3) \\ \frac{1}{4}(1-\xi_2)(1+\xi_3) \\ \frac{1}{4}(1+\xi_2)(1+\xi_3) \end{Bmatrix} \tag{3.36}$$

The shape functions corresponding to 8-noded 2D element are given by,

$$\Psi^{2D} = \begin{Bmatrix} -\frac{1}{4}(1-\xi_2)(1-\xi_3)(1+\xi_2+\xi_3) \\ \frac{1}{2}\left(1-{\xi_2}^2\right)(1-\xi_3) \\ -\frac{1}{4}(1+\xi_2)(1-\xi_3)(1-\xi_2+\xi_3) \\ \frac{1}{2}(1-\xi_2)\left(1-{\xi_3}^2\right) \\ \frac{1}{2}(1+\xi_2)\left(1-{\xi_3}^2\right) \\ -\frac{1}{4}(1-\xi_2)(1+\xi_3)(1+\xi_2-\xi_3) \\ \frac{1}{2}\left(1+{\xi_2}^2\right)(1-\xi_3) \\ -\frac{1}{4}(1+\xi_2)(1+\xi_3)(1-\xi_2-\xi_3) \end{Bmatrix} \tag{3.37}$$

The 3D FEA was performed using the in-house FE code BETA. The Q3D FE analysis is implemented separately in MATLAB.

CHAPTER IV

CONFIGURATIONS

Several slender members with different geometric features (including material distributions) are analyzed with the developed tools. Since the developed tools can only analyze beams which exhibit a mirror symmetry about x_2x_3 plane, all models that are considered do exhibit this symmetry. All models that are analyzed here are categorized into two types based on the geometry and the distribution of materials. The first type of models are the ones in which distribution of material properties does not change along the length of the slender member. Hence these kind of models can be analyzed using both Q3D and Unit Cell methods. The cross sections which are analyzed under this category are: homogeneous isotropic rectangular, inverted T, 3-cell box beam and layered composite beams made of 0^0 and 90^0 deg plies. The second type of models are the ones in which the geometric features change but vary periodically along the length. Since the material properties change along the length, these models can only be analyzed using the Unit Cell method. The plain weave composite laminated beams of different layups are considered under this category. The geometric features, material properties and finite element mesh configurations for each model are presented in the following discussion. For all models in the finite element analysis, 2D quadratic quadrilateral elements for the Q3D method and 3D quadratic hex elements for the Unit Cell method are employed.

A. Slender Members of Type I

The material distribution and the geometry of this type of slender members remain constant along the length. Five different models are analyzed with the geometric features varied from one model to the other. Note that in all Type I models, the 2D

mesh for the Q3D method is structured and composed of quadratic elements. For the Unit Cell method, the same 2D mesh is extruded to obtain one layer of 3D quadratic hex elements. This helps in making comparisons between the deformations predicted from Q3D and Unit Cell methods.

1. Isotropic Rectangular Section

A simple homogeneous beam with rectangular cross section made of isotropic material is analyzed. This model is considered here to compare the predicted effective properties from the current analysis with those from the SOM calculations, which are accurate in this case. The beam geometry and the mesh configuration is shown in Figure 19. The material properties of the isotropic material used are: $E = 10.153e6$ and $\nu = 0.35$. The origin of the coordinate system with respect to which the effective properties are calculated is placed at the area centroid of the cross section.

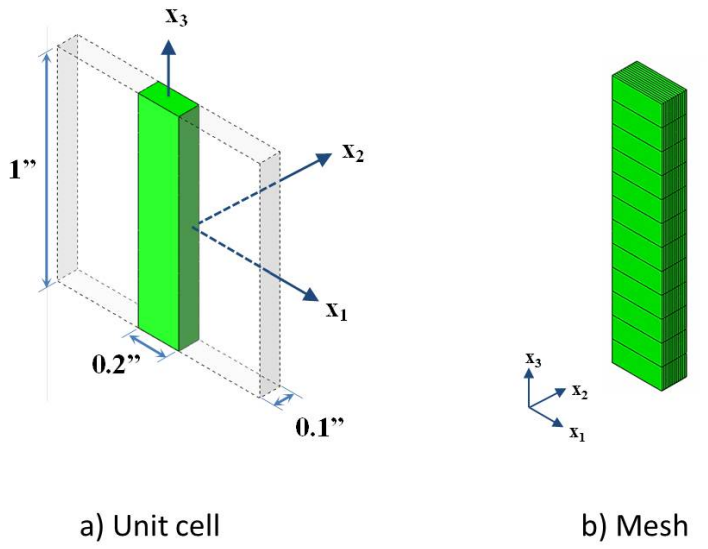

Fig. 19. Isotropic rectangular section

2. Layered Orthotropic Rectangular Section

A four-layered composite beam of rectangular cross section is analyzed. Each ply is made of transversely isotropic material whose properties are: $E_{11} = 22.909e6$, $E_{22} = 1.309e6$, $E_{33} = 1.309e6$, $\nu_{23} = 0.3749$, $\nu_{13} = 0.2412$, $\nu_{12} = 0.2412$, $G_{23} = 0.484e6$, $G_{13} = 0.743e6$, $G_{12} = 0.743e6$. Three different layups, $[0/90]_s$, $[90/0]_s$ and $[(0)_2/(90)_2]$, are considered for the analysis to compare the influence of stacking on the mechanical behavior of the beam. Also for the [0/0/90/90] layup, which shows an extension-flexure coupling behavior, the coupled terms in the effective stiffness matrix are expected to be determined from the current analysis tools. The coordinate system is placed at the area centroid of the cross section for all three layups. The geometry and the mesh configurations are shown in Figure 20.

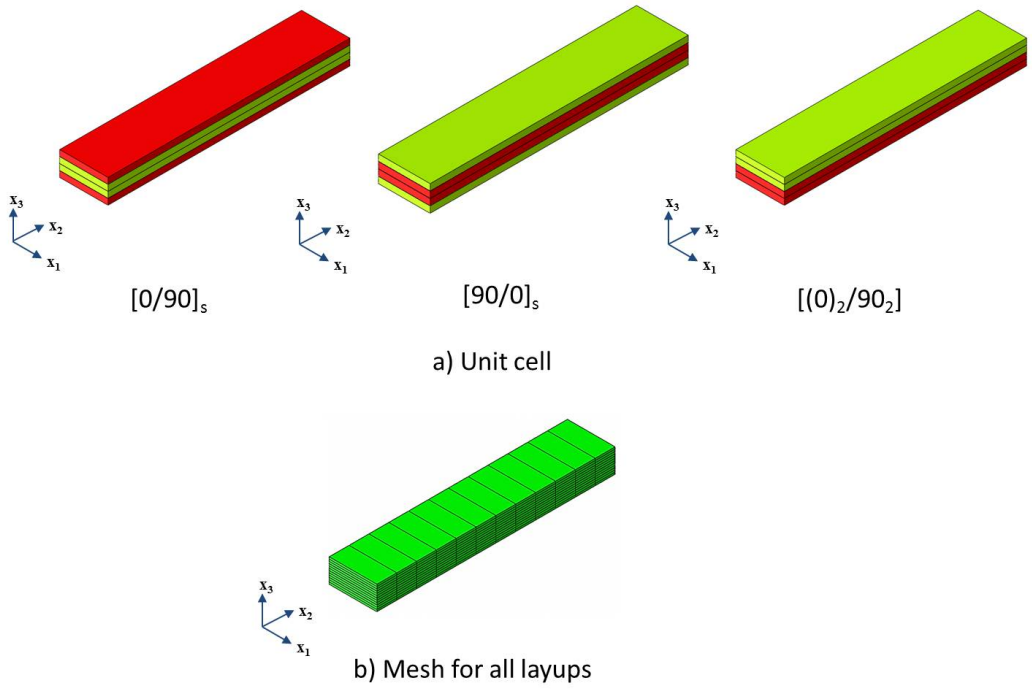

Fig. 20. Layered orthotropic configurations

3. Inverted T-Section

A homogeneous beam with inverted T-section made of isotropic material is considered (see Figure 21). This configuration is taken from [8] where it is analyzed using Variational Asymptotic Beam Sectional Analysis (VABS). Unlike the rectangular section which has two planes of symmetry (x_1x_2 and x_1x_3), the inverted T-section has only one plane of symmetry (x_1x_3). Also the coordinate system is placed with an offset from the area centroid. This offset which gives rise to an extension-flexure coupling term in the effective stiffness matrix helps in determining the robustness of the current analysis tools in predicting the effective properties with respect to a coordinate system placed at any point in the cross section. The material properties used in this model are: $E = 3.0e11$ and $\nu = 0.49$.

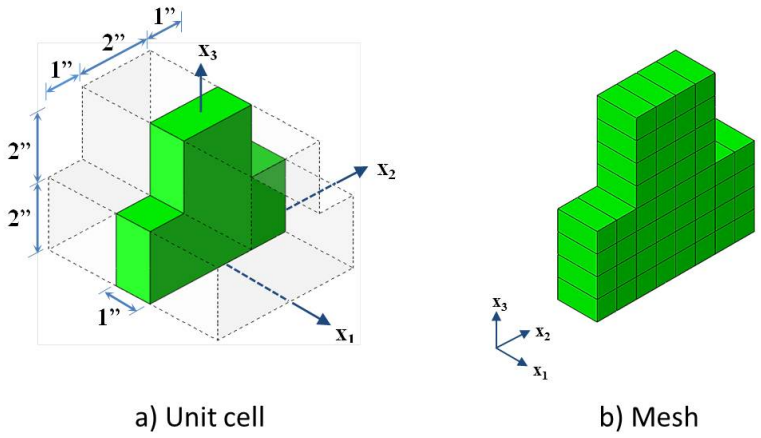

Fig. 21. Isotropic inverted T-section

4. 3-Cell Box Beam Section

A homogeneous 3-cell box beam made of isotropic material shown in Figure 22 is analyzed. The configuration is again taken from [8] for comparison purpose. The cross section is composed of 3 cells of different dimensions. The shear webs are

placed asymmetrically in the cross section. From the SOM calculations using thin wall approximations, it can be expected that the cross section due to asymmetry can give rise to coupling between two shears and the torsion. The coordinate system is placed away from the area centroid of the cross section which results in the coupling between extension and two flexures. The material properties used for this model are: $E = 10.153e6$ and $\nu = 0.35$.

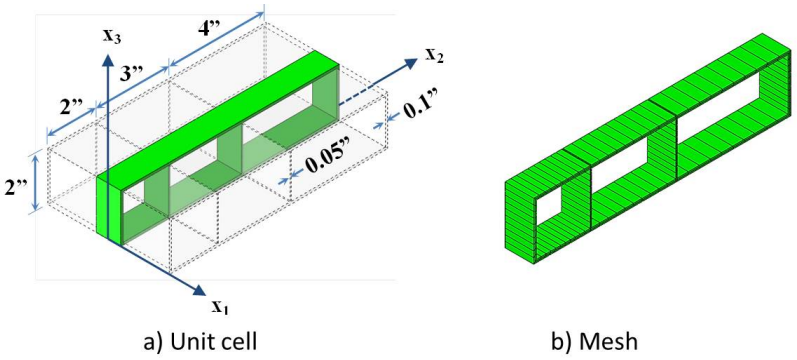

Fig. 22. 3-cell box beam section

5. Wind Turbine Blade Section

A cross section of a wind turbine blade shown in Figure 23 was considered. The section dimensions and material properties are taken from the reference [16]. The section has the shape of S818 airfoil with a chord length of 1m. The shear webs are placed at 15% and 50% chord lengths. The coordinate system is placed at the fore end of the airfoil. Five different materials (see Table II) with various layups are used in different parts of the section (see Figure 23). The skin of the section is made of 5 layers whereas the shear webs are made of 3 layers. The thickness of the skin is 10mm till 15%, 30mm from 15% to 50% and 15mm after 50% of chord length. The thickness of the shear webs are 10mm each. The core material for the shear webs and for the skin till 15% and after 50% of the chord length is made of balsa.

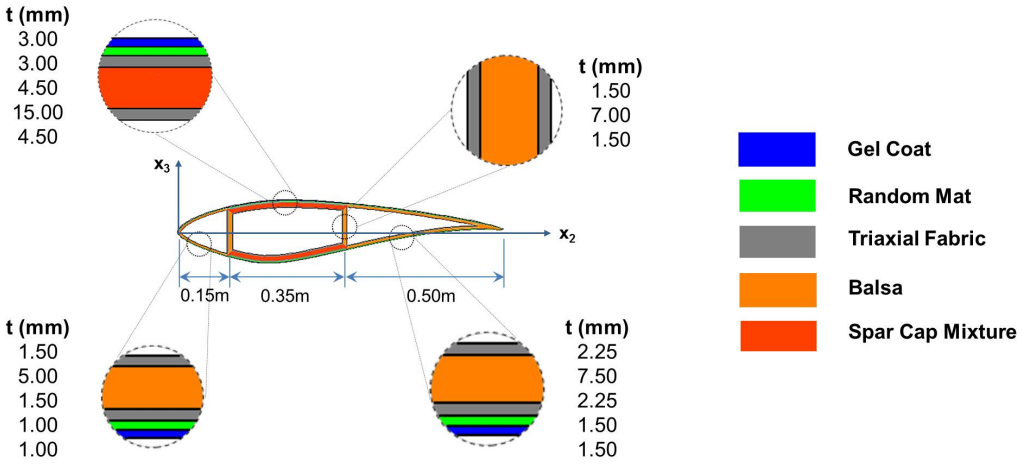

Fig. 23. Section of a wind turbine blade [16]

Table II. Material properties for the wind turbine blade section shown in Figure 23

Material	E_{11} (GPa)	$E_{22} = E_{33}^*$ (GPa)	ν_{23}^*	$\nu_{13} = \nu_{12}$	G_{23}^* (GPa)	$G_{13} = G_{12}$ (GPa)
Gel Coat	3.44	3.44	0.3	0.3	1.38	1.38
Random Mat	9.65	9.65	0.3	0.3	3.86	3.86
Triaxial Fabric	24.2	8.97	0.3	0.39	3.45	4.97
Balsa	2.07	2.07	0.22	0.22	0.14	0.14
Spar Cap Mixture	27.1	8.35	0.3	0.37	3.21	4.7

The core material for the skin between the shear webs (i.e. from 15% to 50% chord length) is made of "Spar Cap Mixture". The Spar Cap Mixture is made of alternate layers of triaxial fabric and uniaxial fabric. It contains 70% of uniaxial fibres and 30% of off-axis fibers [16]. The thicknesses of the layers of materials are slightly altered from those given in the reference for simplicity in modeling of the section. Also the material properties given in the reference were incomplete for 3D analysis since they were obtained from experimental tests and laminated plate theory. Hence

arbitrary (but reasonable) values are chosen for the unreported properties (highlighted with "*" in the superscript in Table II) for the 3D analysis.

B. Slender Members of Type II

This type of slender members have periodic variation of geometry and material distributions along the length. The Unit Cell method can also analyze beams made of periodic geometry and material distributions along the length. However the length of the unit cell for analyzing such beams, should be an integer multiple of the wavelength of the periodicity. The only other restriction the Unit Cell method has is that the unit cell of the beam should have x_2x_3 as a plane of symmetry. Here different layups of plain weave composite beams with varying number of plies and stacking sequences are analyzed. Only one plain weave unit cell along the length of the composite beam are considered here for the analysis.

1. Single Mat - Plain Weave Composite Beam

A single mat of plain weave unit cell with warp and fill tows made of homogeneous transversely isotropic material and the matrix region made of homogeneous isotropic material is considered here. The configuration of the unit cell is shown in Figure 24. A waviness ratio (the ratio of wave length of the warp and fill tows to the thickness

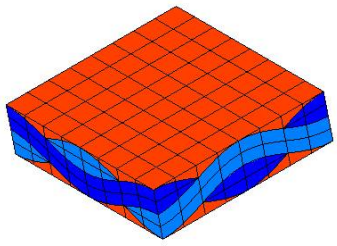

Fig. 24. Single mat plain weave composite beam section

of the mat) of 3 is considered for the analysis. The mat thickness is taken as 1 unit.

2. Multiple Mat - Plain Weave Composite Beam

Multilayered woven composite beam with each layer being a plain weave mat shown in Figure 24. Different configurations with varying number of layers (2, 4 and 10) and stacking sequences (simple and symmetric) are considered. Figure 25 shows unit cells of a two-mat beam with simple and symmetric stacking configurations.

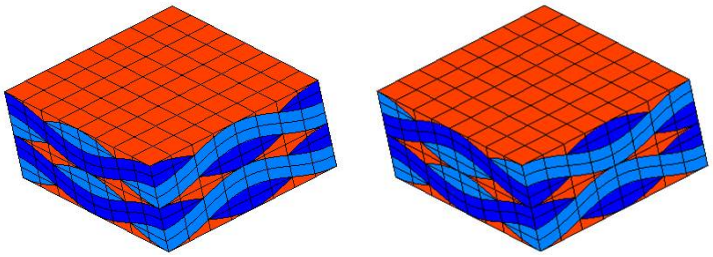

(a) **(b)**

Fig. 25. Two mats plain weave composite beam **(a)** simple stacking **(b)** symmetric stacking

CHAPTER V

RESULTS

The results for various configurations presented in the previous chapter are obtained from the methods developed in the current work. All routines corresponding to the Q3D method are implemented in MATLAB. For the Unit Cell (UC) method, the in-house FE package BETA is used for predicting the deformations for the six fundamental modes. Additional subroutines implemented in MATLAB are used for post processing the FEA output to obtain the effective properties and stress resultants. The obtained results are compared with 3D finite element analysis (3D FEA) of long full length beams, strength of materials (SOM) (only for simple models) and Variational Asymptotic Beam Section Analysis (VABS) [8]. The effective properties from the full length beams are predicted from the strain energies for six modes corresponding to the part of the beam sufficiently away from the ends i.e. only the interior part of the beam. This is done to avoid the influence of end effects on the predicted effective properties. The SOM calculations are done based on the simple 1D models presented in Chapter 1. VABS software was obtained from Dr. Wenbin Yu [8]. The effective properties from all methods are presented in a table format for each cross section. Only the non-zero terms of the effective stiffness matrix are presented in the tables. The VABS-C and VABS-T in the tables refer to VABS Classical and VABS Timoshenko like analyses respectively.

A. Influence of End Effects on Predicted Effective Properties

A long homogeneous beam with rectangular cross section shown in Figure 11 was analyzed for the six deformation modes using simple plane translation and rotation BC's. As discussed in Chapter 3, these plane translation BC's for shear modes constrain

the warping of the end cross section planes and generate end effects. Considering each layer of elements along the length as a single unit cell, effective properties are predicted for all unit cells along the length. Figure 26 shows the variation of the predicted effective properties C_{22} and C_{33} along the length. It can be seen that both properties remained constant in the inner part of the beam but varied significantly near the ends due to end effects. Also the the influence of end effects on C_{22} is much greater than that on C_{33}. The figure also illustrates the validity of the St. Venant's principle which states that the end effects vanish at a distance sufficiently away from the ends.

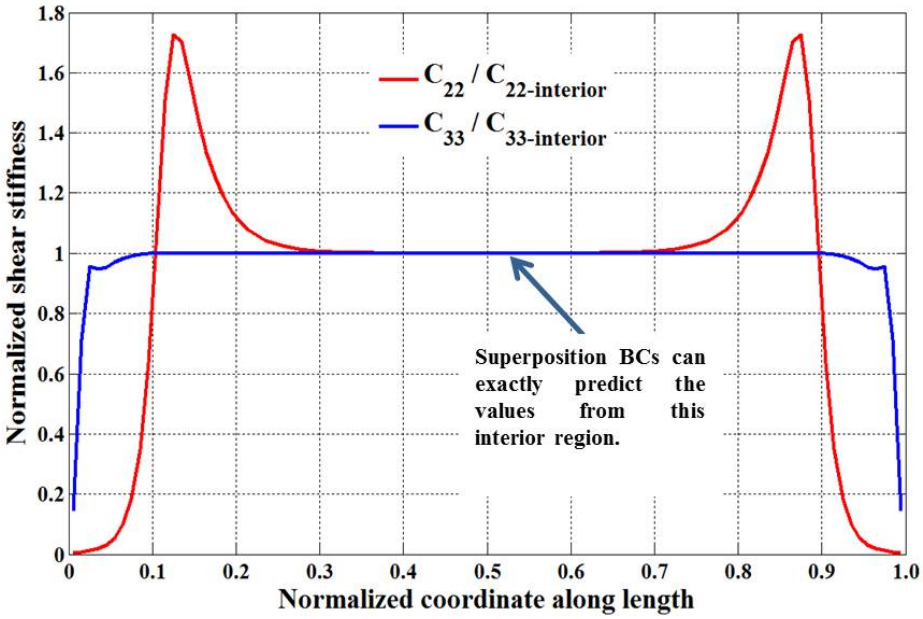

Fig. 26. Variation of the stiffness values C_{22} and C_{33} along the length of a long beam

B. Effective Properties for the Slender Members of Type I

Since the material properties and the geometry are not changing along the length the effective properties depend only on the cross section shape and the material distribution in the cross section.

1. Isotropic Rectangular Section

The cross section has low aspect ratio along x_2 and high aspect ratio along x_3. The coordinate system is placed at the area centroid of the cross section. Since the material is isotropic, the section exhibits symmetry about both the x_2 and x_3 axes. The deformed shapes from the Unit Cell method are shown in Figure 27. The beam constitutive relations predicted using Q3D method and Unit Cell methods are given in Eq. (5.1).

$$\begin{Bmatrix} F_1 \\ M_1 \\ M_2 \\ M_3 \end{Bmatrix} = \begin{bmatrix} 1.0153e6 & 0 & 0 & 0 \\ 0 & 1.1759e3 & 0 & 0 \\ 0 & 0 & 8.4608e4 & 0 \\ 0 & 0 & 0 & 8.4608e2 \end{bmatrix} \begin{Bmatrix} \varepsilon_1 \\ \kappa_1 \\ \kappa_2 \\ \kappa_3 \end{Bmatrix} \tag{5.1a}$$

$$\begin{Bmatrix} F_1 \\ F_2 \\ F_3 \\ M_1 \\ M_2 \\ M_3 \end{Bmatrix} = \begin{bmatrix} 1.0153e6 & 0 & 0 & 0 & 0 & 0 \\ 0 & 5.6334e4 & 0 & 0 & 0 & 0 \\ 0 & 0 & 3.1332e5 & 0 & 0 & 0 \\ 0 & 0 & 0 & 1.1759e3 & 0 & 0 \\ 0 & 0 & 0 & 0 & 8.4608e4 & 0 \\ 0 & 0 & 0 & 0 & 0 & 8.4608e2 \end{bmatrix} \begin{Bmatrix} \epsilon_1 \\ \epsilon_2 \\ \epsilon_3 \\ \kappa_1 \\ \kappa_2 \\ \kappa_3 \end{Bmatrix} \tag{5.1b}$$

Table III gives the properties predicted from various methods. Here, VABS Classical method is similar to the current Q3D method which neglects the contributions from the shear modes and VABS Timoshenko method is similar to the Unit Cell method which accounts for the shear modes. The table shows that the values predicted from Q3D and Unit Cell methods are in excellent agreement with 3D FEA as well as VABS. The SOM predictions for the stiffness values are made following the

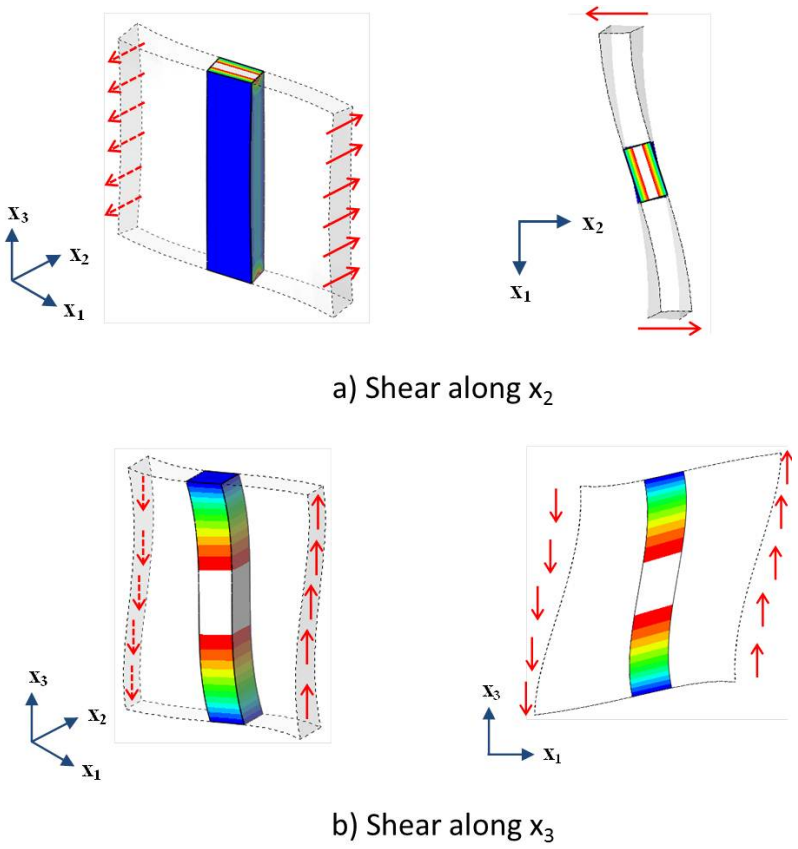

Fig. 27. Shear deformation modes in isotropic rectangular section

simple 1-D models presented in Chapter 1. The simple 1D beam models (both Euler-Bernoulli and Timoshenko) predict that the stresses do not vary along the thickness direction (the direction perpendicular to the direction of shear resultants) of the cross section. Hence they can accurately predict the behavior of beams with cross sections having large height to thickness ratios. They can lead to large errors for the beams having small height to thickness ratios. In the current model, the height to thickness ratio along x_2 is 0.1 (= dimension along x_2/dimension along x_3) whereas along x_3 it is 10 (= dimension along x_3/dimension along x_2). The shear stiffness C_{22} predicted from SOM is 4.5 times larger than the value predicted from 3D FEA. Figure 28 shows the shear stress contours under transverse shear forces F_2 and F_3. The contours un-

Table III. Effective properties for isotropic rectangular section

	Long Beam	Q3D	VABS-C	UC	SOM	VABS-T
C_{11}	1.0153e6	1.0153e6	1.0153e6	1.0153e6	1.0153e6	1.0153e6
C_{22}	5.6334e4	—	—	5.6334e4	3.1333e5	5.5655e4
C_{33}	3.1332e5	—	—	3.1332e5	3.1333e5	3.1333e5
C_{44}	1.1759e3	1.1759e3	1.1759e3	1.1759e3	3.1563e4	1.1759e3
C_{55}	8.4608e4	8.4608e4	8.4608e4	8.4608e4	8.4608e4	8.4608e4
C_{66}	8.4608e2	8.4608e2	8.4608e2	8.4608e2	8.4608e2	8.4608e2

der load F_3 do not vary along x_2 (the thickness direction for the load along x_3) and hence agree with the predictions from SOM. But the contours under load F_2 vary significantly along x_3 (the thickness direction for the load along x_2) and hence the predictions from the SOM fail in this case.

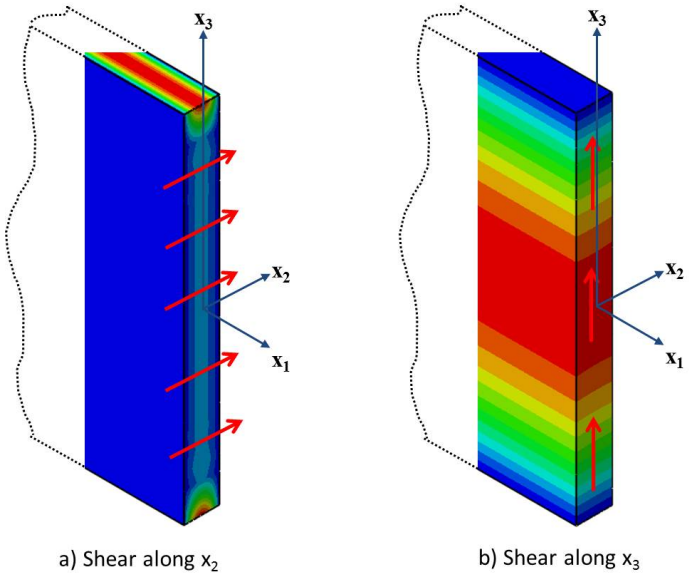

Fig. 28. Shear stress contours under shear loads in isotropic rectangular section

2. Layered Orthotropic Section

Layered orthotropic beam with three different layups, $[0/90]_s$, $[90/0]_s$ and $[(0)_2/(90)_2]$, shown in Figure 20 were analyzed for the effective properties. All layers are of equal thicknesses and made of the same material. The first two layups are balanced symmetric layups whereas the third is an unsymmetric layup. Both symmetric layups do not exhibit any coupling behavior i.e. the off-diagonal terms are zero for both layups. The unsymmetric layup $[(0)_2/(90)_2]$ exhibits extension flexure coupling about the chosen coordinate system. The deformed shapes for various modes predicted from Unit Cell method are shown in Figure 29. Tables IV to VI give the effective properties predicted from various methods. For the symmetric layups, the predictions for all effective properties from all the methods agree well with each other except for C_{33} from SOM approach. The reason for the error in C_{33} from SOM is because, SOM predicts that the stresses do not vary through the thickness which is not the actual behavior seen from 3D analysis. Also, since there are no extension-flexure and shear-flexure coupling terms for the symmetric layups, the locations of the shear center and the weighted centroid are predicted to be at origin of the coordinate system.

Table IV. Effective properties for layered orthotropic $[0/90]_s$ section

	Long Beam	Q3D	VABS-C	UC	SOM	VABS-T
C_{11}	1.2139e6	1.2139e6	1.2139e6	1.2139e6	1.2109e6	1.2139e6
C_{22}	6.1783e4	—	—	6.1783e4	6.1917e4	6.1783e4
C_{33}	4.6465e4	—	—	4.6465e4	5.1125e4	4.6374e4
C_{44}	2.2933e2	2.2933e2	2.2933e2	2.2933e2	1.5488e4	2.2933e3
C_{55}	1.6874e3	1.6874e3	1.6874e3	1.6874e3	1.6841e3	1.6874e3
C_{66}	1.0113e5	1.0113e5	1.0113e5	1.0113e5	1.0091e5	1.0113e5

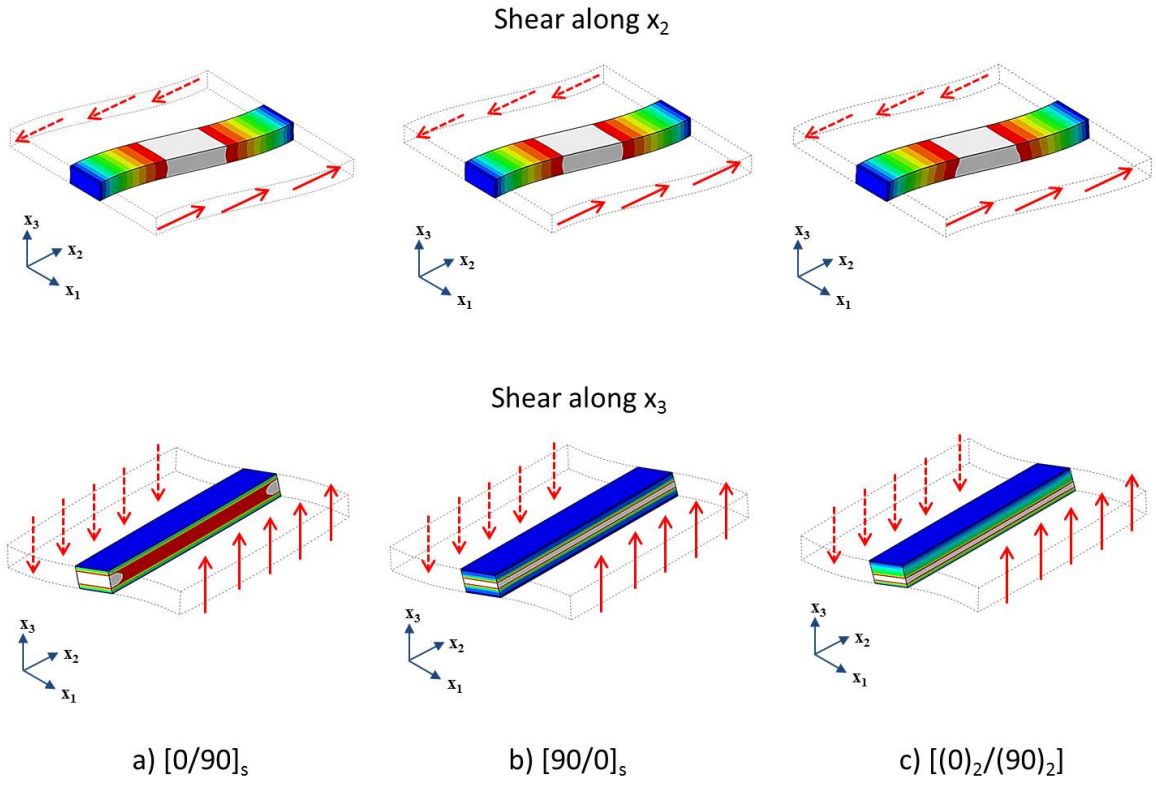

Fig. 29. Shear deformations in the layered orthotropic rectangular section

The unsymmetric layup, $[(0)_2/(90)_2]$, exhibits coupling behavior between extension and flexure (C_{15}) as well as shear and torsion (C_{24}). From Table VI, the properties corresponding to extension and flexure are the same from both Q3D and Unit Cell methods. But the torsion stiffness C_{44} predicted from Q3D differs from that predicted using Unit Cell method by about 10%. The reason for this is because of the coupling behavior of the beam between shear and torsion. Since Q3D cannot accommodate shear deformation behavior, the predictions for the torsion deformation are not accurate. Hence one should be careful in using Q3D because it can lead to incorrect predictions of the properties for the beams which show coupling behavior with shear modes. The predictions from the Unit Cell method for the coupled terms matched well with 3D FEA as well as VABS Timoshenko methods. Figure 30 shows

Table V. Effective properties for layered orthotropic $[90/0]_s$ section

	Long Beam	Q3D	VABS-C	UC	SOM	VABS-T
C_{11}	1.2139e6	1.2139e6	1.2139e6	1.2139e6	1.2109e6	1.2139e6
C_{22}	6.1780e4	—	—	6.1780e4	6.1917e4	6.1780e4
C_{33}	4.1131e4	—	—	4.1131e4	5.1125e4	3.9923e4
C_{44}	2.3145e2	2.3145e2	2.3145e2	2.3145e2	1.5488e4	2.3145e2
C_{55}	3.3477e2	3.3477e2	3.3477e2	3.3477e2	3.3408e2	3.3477e2
C_{66}	1.0113e5	1.0113e5	1.0113e5	1.0113e5	1.0091e5	1.0113e5

the two coupled deformation modes, extension-flexure and shear-torsion, of the unsymmetric layup. The presence of these coupling behaviors indicate that the origin of the coordinate system is away from both weighted centroid and the shear center. The predicted locations of weighted centroid and shear centers for the unsymmetric layup are $(\xi_{2c} = 0, \xi_{3c} = -0.0220)$ and $(\xi_{2sc} = 0, \xi_{3sc} = 0.0216)$ respectively. These predictions were with in 1.4% when compared to VABS.

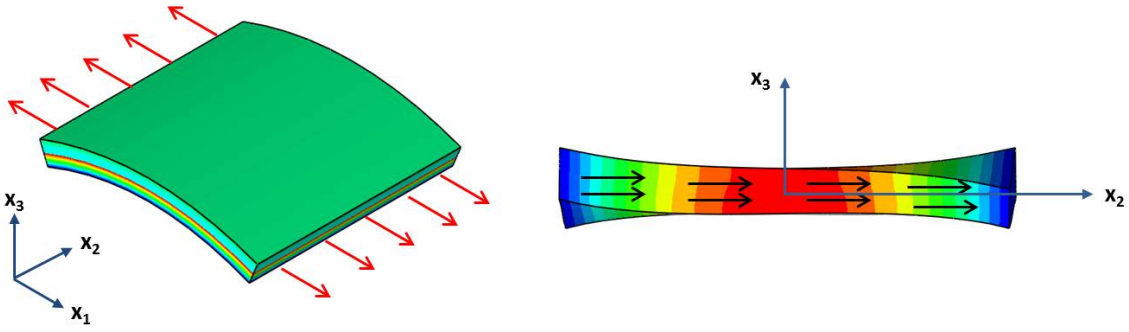

Fig. 30. Coupled deformation modes in $[(0)_2/(90)_2]$ layered beam

Table VI. Effective properties for layered orthotropic $[0_2/90_2]$ section

	Long Beam	Q3D	VABS-C	UC	SOM	VABS-T
C_{11}	1.2127e6	1.2127e6	1.2127e6	1.2127e6	1.2109e6	1.2127e6
C_{15}	-2.7038e4	-2.7038e4	-2.7038e4	-2.7038e4	—	-2.7038e4
C_{22}	6.1406e4	—	—	6.1406e4	6.1917e4	6.1406e4
C_{24}	-1.3287e3	—	—	-1.3287e3	—	-1.3287e3
C_{33}	4.8652e4	—	—	4.8652e4	5.1125e4	4.7495e4
C_{44}	2.5913e2	2.3038e2	2.3038e2	2.5913e2	1.5488e4	2.5913e2
C_{55}	1.0105e3	1.0108e3	1.0105e3	1.0105e3	1.0091e3	1.0105e3
C_{66}	1.0103e5	1.0103e5	1.0103e5	1.0103e5	1.0091e5	1.0103e5

3. Isotropic Inverted T-Section

The inverted T-section beam is homogeneous and made of isotropic material. The coordinate system is placed away from the area centroid of the cross section. Also the cross section has only one plane of symmetry unlike the isotropic rectangular section which has both in-plane axes as planes of symmetry. The shear deformation modes predicted using the Unit Cell method are shown in Figure 31 along with the shear stress contours. The warping of the cross section can be seen to be predicted accurately for both the shear modes since no end effects are seen in the shear stress contours. The effective properties predicted from various methods are shown in Table VII.

Note that the SOM calculations for the shear modes are performed assuming the cross section is divided into different rectangular subregions as shown in Figure 32. The shear forces are distributed among the subregions assuming that each subregion takes the shear load proportional to its area. The shear stress distributions in each

rectangular subregion is considered as parabolic assuming that one region is not interacting with the other.

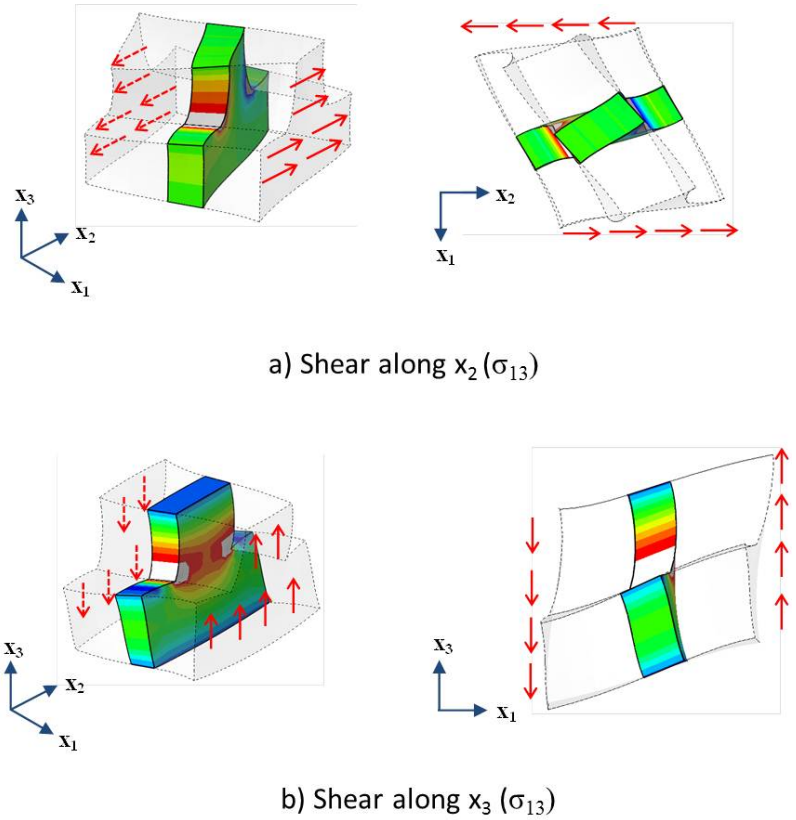

Fig. 31. Shear deformation modes in inverted T-section

The effective properties from all methods agree exactly for the extension and flexure modes. The shear properties from SOM are different because of the assumptions made on the distribution of shear stress under shear loads. The beam exhibits two coupling modes, extension-flexure (C_{15}) and shear-torsion (C_{24}). Both the terms arise due to the asymmetry in the cross section and the offset in the coordinate system from the area centroid. The extension and flexure properties from Q3D and Unit Cell methods agree with each other but the torsional properties are significantly different because of the coupling between shear and torsion modes which Q3D neglects.

Table VII. Effective properties for inverted T-section

	Long Beam	Q3D	VABS-C	UC	SOM	VABS-T
C_{11}	3.6003e12	3.6000e12	3.6000e12	3.6003e12	3.6000e12	3.6000e12
C_{15}	6.0004e12	6.0000e12	6.0000e12	6.0004e12	6.0000e12	6.0000e12
C_{22}	0.8784e12	—	—	0.8784e12	1.0000e12	0.8765e12
C_{24}	-1.2757e12	—	—	-1.2757e12	-1.6667e12	-1.2692e12
C_{33}	0.8118e12	—	—	0.8118e12	1.0000e12	0.8091e12
C_{44}	3.3484e12	1.4870e12	1.4880e12	3.3484e12	6.0000e12	3.3260e12
C_{55}	1.4400e13	1.4400e13	1.4400e13	1.4400e13	1.4400e13	1.4400e13
C_{66}	3.6000e12	3.6000e12	3.6000e12	3.6000e12	3.6000e12	3.6000e12

The locations of the weighted centroid and the shear center are predicted to be at $(\xi_{2c} = 0, \xi_{3c} = 1.6667)$ and $(\xi_{2sc} = 0, \xi_{3sc} = 1.4522)$ respectively. These predictions were with in 0.3% when compared to VABS.

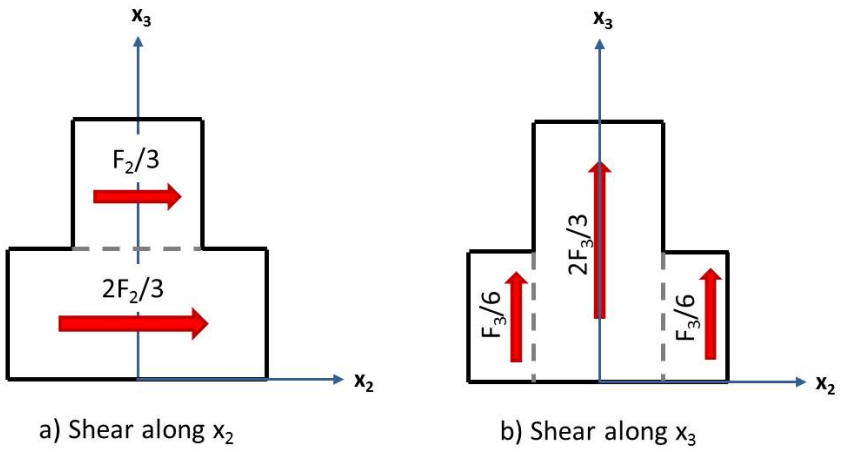

Fig. 32. SOM approximation for shear stress distribution in inverted-T Section

4. 3-Cell Box Beam Section

The 3-cell box beam section resembles an idealized homogeneous multi-celled wind turbine blade. The coordinate system is placed away from the area centroid of the cross section to predict the coupling terms. The cross section has only one plane of symmetry since the shear webs are positioned asymmetrically along x_2. The shear deformation modes predicted from the Unit Cell method are shown in Figure 33 along with the shear stress contours. The effective properties from various methods

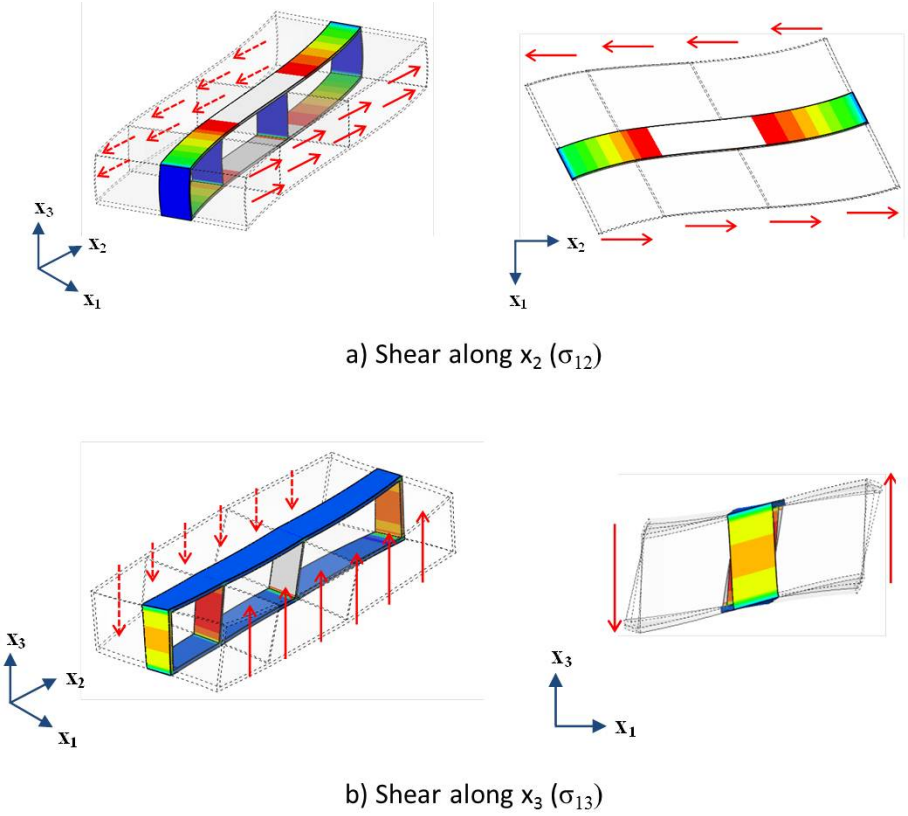

Fig. 33. Shear deformation modes in 3-cell box beam section

are shown in Table VIII. The SOM calculations for the shear modes are performed assuming the thin-wall assumption i.e. assuming that the flanges cannot take shear loads in the thickness direction. The cross section has more non-zero coupling terms

than the inverted T-section because of the offset in the coordinate system along both the in-plane axes. This offset from the area centroid resulted in non-zero C_{15}, C_{16} and C_{56}. The effective properties from all methods again agree exactly for extension and flexure modes. Because of the coupling between torsion and shear mode corresponding to F_2, the torsion properties from Q3D and Unit Cell methods are significantly different from each other. The locations of the weighted centroid and the shear center are predicted to be at $(\xi_{2c} = 4.4231, \xi_{3c} = 1.0000)$ and $(\xi_{2sc} = 4.3535, \xi_{3sc} = 1.0000)$ respectively. These predictions were with in 0.01% when compared to VABS.

Table VIII. Effective properties for 3-cell box beam section

	Long Beam	Q3D	VABS-C	UC	SOM	VABS-T
C_{11}	2.3758e7	2.3758e7	2.3758e7	2.3758e7	2.3758e7	2.3758e7
C_{15}	2.3758e7	2.3758e7	2.3758e7	2.3758e7	2.3758e7	2.3758e7
C_{16}	-1.0508e8	-1.0508e8	-1.0508e8	-1.0508e8	-1.0508e8	-1.0508e8
C_{22}	6.1431e6	—	—	6.1431e6	5.6400e6	6.1437e6
C_{24}	-6.1435e6	—	—	-6.1435e6	-5.6400e6	-6.1437e6
C_{33}	1.4305e6	—	—	1.4305e6	1.8800e6	1.4305e6
C_{34}	6.2276e6	—	—	6.2276e6	—	6.2275e6
C_{44}	5.3585e7	2.0329e7	2.0329e7	5.3585e7	1.8800e7	5.3585e7
C_{55}	4.1747e7	4.1747e7	4.1747e7	4.1747e7	4.1747e7	4.1747e7
C_{56}	-1.0508e8	-1.0508e8	-1.0508e8	-1.0508e8	-1.0706e8	-1.0508e8
C_{66}	6.6633e8	6.6633e8	6.6633e8	6.6633e8	6.5626e8	6.6633e8

5. Wind Turbine Blade Section

The section is made of S818 airfoil (chord length = $1m$) with different layers of materials. There are two shear webs at 15% and 50% chord lengths (see Figure 23).

The section is considered from reference [16]. The coordinate system is placed at the fore end of the cross section. The calculated properties are shown in Table IX. Since the cross section is complex, the SOM calculations were not performed.

Table IX. Effective properties for the wind turbine blade section

	Long Beam	Q3D	VABS-C	UC	VABS-T
C_{11}	6.5606e8	6.5599e8	6.5605e8	6.5606e8	6.5605e8
C_{15}	6.8113e6	6.8068e6	6.8076e6	6.8113e6	6.8076e6
C_{16}	-2.5161e8	-2.5160e6	-2.5162e8	-2.5161e8	-2.5162e8
C_{22}	8.5839e7	—	—	8.5839e7	8.5841e7
C_{23}	4.2060e6	—	—	4.2060e6	4.1985e6
C_{24}	2.9360e5	—	—	2.9360e5	2.9287e5
C_{33}	1.2262e7	—	—	1.2262e7	1.2238e7
C_{34}	3.5724e6	—	—	3.5724e6	3.5706e6
C_{44}	2.7616e6	1.7096e6	1.7103e6	2.7616e6	2.7623e6
C_{55}	4.6406e6	4.6403e6	4.6404e6	4.6406e6	4.6404e6
C_{56}	-3.8976e6	-3.8969e6	-3.8972e6	-3.8976e6	-3.8972e6
C_{66}	1.2224e8	1.2224e8	1.2224e8	1.2224e8	1.2224e8

The cross section gave several coupling terms: extension-flexure (C_{15} and C_{16}), shear-shear (C_{23}), shear-torsion (C_{24} and C_{34}) and flexure-flexure (C_{56}). The results from the Unit Cell method showed excellent agreement with those from the 3D analysis of a long beam as well as from VABS Timoshenko-like analysis. The results from Q3D and VABS classical analyses showed good agreement for extension and flexure properties but not for torsion properties. The torsional property C_{44} from Q3D differed from the 3D analysis of a long beam by about 38%. The reason for this significant error is because of the presence of coupling between torsion and shear

which the Q3D could not capture. The predicted location of weighted centroid is at ($\xi_{2c} = 0.3835, \xi_{3c} = 0.0104$) whereas that of shear center is at ($\xi_{2sc} = 0.2951, \xi_{3sc} = 0.0110$). These predictions agreed well with those from VABS Timshenko like analysis (error of about 0.14%).

C. Effective Properties for the Slender Members of Type II

The second type of slender members have geometry and/or material properties varying periodically along the length. Note that most of the existing cross section analysis tools are based on analyzing a characteristic 2D cross section of a beam. Hence they cannot capture the behavior of the beams which have varying geometric features along the length since no single cross section is characteristic in such cases. The Q3D method also fails in this context because of the same reason.

The Unit Cell method however can analyze such cross sections since the variation along the length is periodic. The length of the unit cell in such cases can be considered as one wavelength (or a multiple of it) corresponding to the periodicity in the geometric features. Plain weave woven-composite beams which fall under this category of slender members are considered here for the analysis. The following models represent idealized configurations of plain weave composites. Also only one unit cell is considered in the cross section of the beam for simplicity in illustrating the capabilities of the current tools. In general several unit cells span the cross section since the dimension of each unit cell is much smaller compared to the typical dimensions of composite beams. Since no available analysis tool can analyze these slender members, the results are validated only by comparison with the interior region of 3D FEA of the long beam composed of several unit cells along the length to avoid the end effects.

1. Beams Made of a Single Plain Weave Mat

A single mat composite beam shown in Figure 24 was analyzed using the Unit Cell method for the six deformation modes. The coordinate system was placed at the geometric center of the unit cell. The deformed configurations of the unit cell under the six deformation modes are shown in Figure 34.

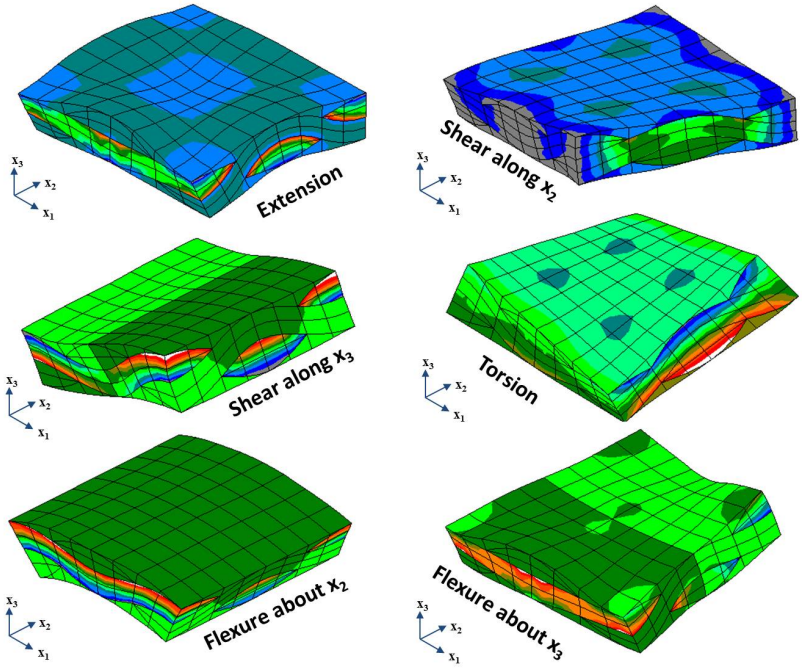

Fig. 34. Fundamental deformations modes of single mat plain weave composite beam

The effective properties for this configuration were predicted similar to the previous models i.e. using the strain energy equivalence principle of the homogenization scheme. The predicted effective properties are shown in Table X. The results matched exactly with those from the long beam analysis. The unit cell, due to asymmetry about the x_1x_2 plane, exhibits a coupling behavior between shear along x_2 and the torsion mode which resulted in non-zero C_{24} term. This coupling term leads to the prediction of shear center to be at $(\xi_{2sc} = 0.0, \xi_{3sc} = -0.0390)$.

Table X. Effective properties for single mat plain weave composite beam

	Single Mat
C_{11}	7.1138e10
C_{22}	1.1722e10
C_{24}	4.5663e8
C_{33}	2.2026e10
C_{44}	2.6374e9
C_{55}	3.4704e9
C_{66}	5.3289e10

2. Beams Made of Multiple Plain Weave Mats

Laminated composite structures are usually composed of several mats to attain the required stiffness and strength properties. Composite beams made of two, four and ten plain weave mats with different stacking sequences were analyzed for the effective stiffness properties (see Figure 25). The different stacking sequences here correspond to simple and symmetric stacking. The symmetric stacking does have x_1x_2 as a plane of symmetry whereas the simple stacking does not. Hence symmetrically stacked configurations exhibit no coupling behavior whereas the simply stacked configurations, similar to the single mat case discussed previously, show coupling between shear and torsion. The deformed shapes of the unit cells with two-mats are shown in Figure 35.

The predicted effective properties for all configurations are shown in Table XI. All values are in excellent agreement (maximum error of 0.001%) with the ones obtained from the long beam analyses (not shown in the table). It can be seen that the term corresponding to shear-torsion coupling C_{24} is non-zero only for the simply stacked configurations. The prediction of the location of shear center for simply stacked two-

mat, four-mat and ten-mat configurations are ($\xi_{2sc} = 0.0, \xi_{3sc} = -0.0890$), ($\xi_{2sc} = 0.0, \xi_{3sc} = -0.1420$) and ($\xi_{2sc} = 0.0, \xi_{3sc} = -0.1810$) respectively.

The effective properties in general are sensitive to the stacking sequence. For example consider the effective properties of the two-mat beam. The stiffness terms C_{11}, C_{33}, C_{55} and C_{66} changed significantly from simple to symmetric stacking with the maximum change observed in C_{66} of about 18%. The out of plane transverse shear stiffness C_{33} showed a change of about 13%. Similar trends are observed in four-mat and ten-mat beams. These models illustrate the importance of the stacking sequence in the design of layered woven composite beams. Since the shear stiffness properties of the finitely thick woven composite beams were not investigated much in the literature, the current approach proves to be a powerful tool since it captures the detailed deformations with accuracy equivalent to full 3D FEA.

Table XI. Effective properties for multiple mat plain weave composite beams

	Simple	Symmetric	Simple	Symmetric	Simple	Symmetric
C_{11}	1.5189e11	1.7152e11	3.1231e11	3.6550e11	7.9352e11	9.4729e11
C_{22}	2.3491e10	2.3373e10	4.6627e10	4.5857e10	1.0384e11	1.0045e11
C_{24}	2.1022e9	0.0	6.6032e9	0.0	1.8750e10	0.0
C_{33}	1.4943e10	1.6925e10	3.5298e10	3.9536e10	9.2495e10	1.0373e11
C_{44}	1.9216e10	1.9930e10	8.0517e10	8.7398e10	2.9534e11	3.3230e11
C_{55}	4.9672e10	4.4994e10	4.1052e11	4.3389e11	6.5240e12	7.5383e12
C_{66}	1.1539e11	1.3639e11	2.3946e11	2.9254e11	6.1164e11	7.6172e11

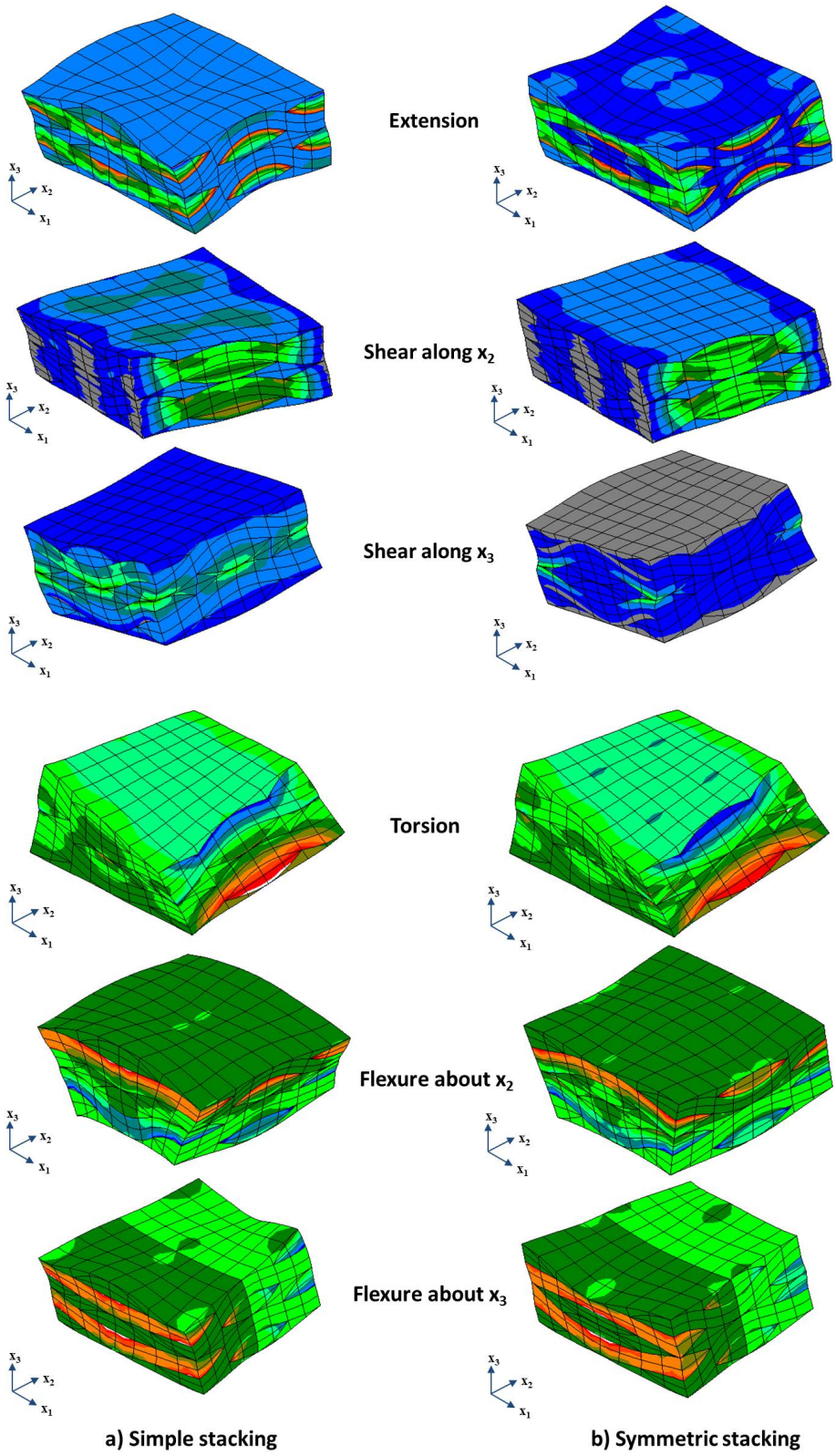

Fig. 35. Fundamental deformations modes of two mat plain weave composite beams simple vs symmetric

CHAPTER VI

CONCLUSIONS AND FUTURE WORK

A. Conclusions

Slender structural members such as wind turbine blades can be accurately modeled using beam models. Wind turbine blades have complex cross section shapes and are made of various composite layups along the length. Hence simple 1D models like uniaxial bar, St. Venant's torsion rod, Euler-Bernoulli and Timoshenko models fail to accurately predict the behavior of wind turbine blades.

The formulation for a generalized beam model is derived which can analyze any slender member with arbitrary cross sections subjected to any combination of beam loads i.e. extension, shears, torsion and flexures. To employ the generalized beam theory for any slender member the corresponding effective section properties need to be obtained. Several cross section analysis techniques existing in the literature were based on various assumptions which in some cases lead to significant errors. The accuracy of the prediction of the mechanical behavior of blades using beam models depends on the accuracy in the prediction of the effective section properties. A homogenization technique based on strain energy equivalence is presented for accurate predictions of effective section properties. The technique requires the calculation of detailed 3D deformations for the six fundamental modes of the beams.

The 3D deformations corresponding to six fundamental modes can be obtained by analyzing a long beam. For accurate predictions, this approach can be expensive especially for complex cross sections. To reduce the computational effort in predicting the deformations corresponding to the six fundamental modes, two new methods - Quasi-3D and Unit Cell - are presented. The Quasi-3D method can analyze extension,

torsion and flexure of beams which do not show coupling behavior with the shear modes. This method is useful for predicting the effective properties for the generalized Euler-Bernoulli beam model. The Unit Cell method on the other hand predicts the deformations corresponding to all six fundamental modes for any slender members that have x_2x_3 as a plane of symmetry. The Quasi-3D method is implemented in MATLAB whereas the Unit Cell method is implemented using the in-house finite element code BETA.

Several models with different geometric features were analyzed for the effective properties using the deformations predicted from Q3D and Unit Cell methods. The results were compared with the 3D FEA of the long beam, Strength of Materials and VABS approaches. Excellent agreement was seen in the predicted properties when compared with the full 3D analysis for all cross sections.

B. Future Work

The homogenization technique based on strain energy equivalence works for any slender members. However the boundary conditions (BC's) derived in the current work for the Unit Cell method can only analyze the slender members which have x_2x_3 as a plane of symmetry. Hence efforts are in progress in developing a general set of BC's which can analyze the slender members which do not have this symmetry. An example of slender members that fall under this category are ones made of plies oriented in directions other than 0 and 90 degrees.

The current work discusses only the static analysis of slender members. An important extension for the current work would be to analyze the structural dynamic behavior of slender members of arbitrary cross sections. For dynamic analysis, along with the effective stiffness properties, effective inertia properties have to be deter-

mined. Dynamic analysis of wind turbine blades is extremely important because all loads that act on the blades under normal operational conditions vary severely with time. Full 3D FEA analysis in such a case would be impractical and the beam models similar to the ones developed in the current work can again prove to be highly powerful and efficient tools.

Also the BC's developed for the unit cell method can be extended to analyze unidirectional and woven composite laminated plates and shells. The current approach can prove to be accurate and efficient especially in predicting the shear behavior of thick composite plates and shells.

REFERENCES

[1] J. R. Wright and J. E. Cooper, *Introduction to Aircraft Aeroelasticity and Loads*, vol. 1, 1st ed. Hoboken, New Jersey: John Wiley & Sons Ltd., 2007.

[2] H. Chen, W. Yu and M. Capellero, "A Critical Assessment of Computer Tools for Calculating Composite Wind Turbine Blade Properties," *Wind Energy*, vol. 13, pp. 497–516, 2009.

[3] B. Resor, J. Paquette, D. Laird and D. T. Griffith, "An Evaluation of Wind Turbine Blade Cross Section Analysis Techniques," in *51st AIAA/ASME/ASCE/AHS/ASC Structures, Structural Dynamics, and Materials Conference*, Orlando, Florida, American Institute of Aeronautics and Astronautics, Inc., April, 2010.

[4] D. J. Lekou and T. P. Philippidis, "PRE- and POST-THIN: A Tool for the Probabilistic Design and Analysis of Composite Rotor Blade Strength," *Wind Energy*, vol. 12, pp. 676–691, 2009.

[5] G. S. Bir, "Computerized Method for Preliminary Structural Design of Composite Wind Turbine Blades," *Journal of Solar Energy Engineering*, vol. 123, pp. 372–381, 2001.

[6] M. H. Hansen, "Aeroelastic Stability Analysis of Wind Turbines Using an Eigen Value Approach," *Wind Energy*, vol. 7, pp. 133–143, 2004.

[7] D. J. Malcolm and D. Liard, "Extraction of Equivalent Beam Properties for Blade Models," *Wind Energy*, vol. 10, pp. 135–157, 2007.

[8] D. H. Hodges, *Nonlinear Composite Beam Theory*, Progress In Aeronautics and Astronautics, vol. 213, 1st ed. Reston, Virginia: American Institute of Aeronautics and Astronautics, Inc., 2006.

[9] Y. Jonnalagadda and J. D. Whitcomb "Calculation of Effective Section Properties for Wind Turbine Blades," in *52nd AIAA/ASME/ASCE/AHS/ASC Structures, Structural Dynamics, and Materials Conference*, Denver, Colorado, American Institute of Aeronautics and Astronautics, Inc., April, 2011.

[10] W. Michael Lai, D. Rubin and E. Krempl, *Introduction to Continuum Mechanics*, 3rd ed. Burlington, Massachusetts: Butterworth-Heinemann, 1999.

[11] N. I. Muskhelishvili, *Some Basic Problems of Mathematical Theory of Elasticity*. Groningen, Netherlands: P. Noordhoff, 1963.

[12] F. Gruttman and W. Wagner, "Shear Correction Factors in Timoshenko's Beam Theory for Arbitrarily Shaped Cross-Sections," *Computational Mechanics*, vol. 27, pp. 199–207, 2001.

[13] B. V. Shankar and R. V. Marrey, "A Unit Cell Model for Textile Composite Beams for Predicting Stiffness Properties," *Composites Science and Technology*, vol. 49, pp. 61–69, 1993.

[14] J. D. Whitcomb, C. D. Chapman and X. Tang, "Derivation of Boundary Conditions for Micromechanics Analysis of Plain and Satin Weave Composites," *Journal of Composite Materials*, vol. 34, pp. 724–747, 2000.

[15] J. N. Reddy, *An Introduction to the Finite Element Method*, 3rd ed. New Delhi, India: Tata McGraw Hill Education Pvt. Ltd., 2005.

[16] D. A. Griffin, "WindPACT Turbine Design Scaling Studies Technical Area 1 - Composite Blades for 80- to 120-Meter Rotor," *National Renewable Energy Laboratory Subcontractor Report*, NREL/SR-500-29492, pp. 5–8, 2001.

VITA

Yellavenkatasunil Jonnalagadda began his undergraduate study in Aerospace Engineering at Indian Institute of Technology Kanpur (IITK) in August of 2005 and graduated with a Bachelor of Technology degree in May of 2009. He began his Master's in Aerospace Engineering at Texas A&M University in August of 2009 and plans to graduate in August of 2011.

Department Address:

Texas A&M University

Department of Aerospace Engineering

H.R. Bright Building, Rm. 701, Ross Street - TAMU 3141

College Station TX, 77843-3141

Phone: (979)209-9201

Email: ysunil@tamu.edu; suniljyv.87@gmail.com

The typist for this thesis was Yellavenkatasunil Jonnalagadda.